

Interactive comment on “Re-examining the 4.2 ka BP event in foraminifer isotope records from the Indus River delta in the Arabian Sea” by Alena Giesche et al.

A. Sinha (Referee)

asinha@csudh.edu

Received and published: 1 October 2018

*Staubwasser et al back in 2003 published an influential paper entitled ‘Climate change at the 4.2 ka BP termination of the Indus valley civilization and Holocene south Asian monsoon variability’. The paper generated a lot of interest and if I am not mistaken, was the first attempt of its kind, to reconstruct variations in Indus river discharge, and thereby, the hydroclimatic history of the region, where the Indus valley civilization emerged, prospered and declined. Fast forward 15 years, Giesche et al manuscript “Re-examining the 4.2 ka BP event in foraminifer isotope records from the Indus River delta in the Arabian Sea” seeks to confirm and improve upon the results from the original study. A salient and an important aspect of this manuscript is that the authors have attempted to reconstruct changes in both summer and winter Indian monsoon by adding new data through the stable oxygen and carbon isotopes analyses of two additional foraminiferal species over a targeted interval from 3.4 to 5.0 ka. They have presented their findings in the context of societal changes that occurred in this region. Additionally, their new data is a step towards a better dynamical understanding of the 4.2 ka event in the Indian subcontinent. Both are critical and important objectives. The paper is well written but its presentation could be further improved (see below). Authors are suitably careful in interpreting the proxy data. The conclusions are reasonably well supported by data and the necessary caveats are clearly noted. I, therefore, highly recommend this manuscript to be published in *Climate of the Past* with some modest revisions.*

We thank Ashish Sinha for taking the time to review our manuscript and provide constructive feedback.

I have outlined my suggestions below that I hope authors will find useful in further improving the ‘scientific and presentation qualities’ of their manuscript.

Manuscript Length: First, I encourage authors to substantially reduce the length of this manuscript. A shortened/concise manuscript will greatly improve its readability. While the authors can decide how to best approach this, I would suggest that figures # 4, 6, and perhaps 7 (and associated discussions) can be easily moved into the supplementary section. Also, aren’t Figures # 3 and 5 somewhat redundant? Can they be merged as a single figure?

We agree that some of the figures can be consolidated. We have now merged figures 3,5, and 7 (the resulting figure is now called figure 3). We have tried to make the language more precise throughout the manuscript to improve the readability, and have removed some redundancies. These changes can be viewed in the revised version of the manuscript, at the end of this file.

Figures Presentation: Figure 1: Fonts are too small particularly on panels b and c. Figure 2c has multiple shades for each species. Are different shades representing sediment trap data for different depths? It is not clear from the figure caption.

The font size has been enlarged for Figure 1. You are correct that the various shadings in Figure 2c show different trap data (deep v. shallow traps). This information has been added to the figure caption.

Figures # 3, 5, 7, 9, and 10: Loess smoothed curves are shown along with the raw data (is that correct?). The latter is shown as scatter plots, which is fine if the goal is to show the effectiveness of Loess smoothing but not very intuitive if one wishes to see the evolution of higher frequency variability in time series. I suggest perhaps one figure with scatter plot can be shown to demonstrate the idea of Loess smoothing and the rest of the figures can be more conventional (i.e., line plots) superimposed by smoothed curves.

We agree that line plots show important information about the raw data over time, therefore we have included lines for the plots in figure 3 (previously split into figures 3/5/7). We have also included lines for figures 7 & 8 (previously called 9 & 10).

Statistical Treatment I would also recommend that authors present foraminifera isotope data as z-scores or anomalies from the mean (that is of course, after initially presenting raw data). This is particularly useful as comparisons are made across the different species and proxy records.

We agree that z-scores can be a useful way of presenting the data and its variability in comparison to other proxies. Because our data and the comparisons are mainly based on $\delta^{18}\text{O}$, we think that the original units of the records are more informative for the reader. Instead, we have uploaded the raw data file, and readers are encouraged to re-plot the data as z-scores if it is useful for their purposes.

Authors have reported the results of several statistical tests in this manuscript. It is not clear whether the statistics were performed on interpolated or raw data. This needs some clarification. What is the average temporal resolution of non-interpolated isotope data? A critical information that I could not find in the manuscript.

We recognize that our original description of the statistical tests did not clarify these important points, and have improved the relevant sections. All statistical tests (t-tests, correlations, SiZer analysis) were performed on non-interpolated raw data (missing depths were ignored). We have now included “n” number of data points for the t-tests, and the p value for the correlation in the Results section. The loess smoothing was generated purely for visualization purposes, and we use a smoothing window/span equivalent to 210/2426 (where 210 represents the years of the smoothing window and 2426 represents the total number of years covered by the dataset). The average temporal resolution of the non-interpolated data is 18 years/cm, with a range of 12-29 years.

Revised manuscript below.

1 **Re-examining Indian winter and summer monsoon strength over the 4.2 ka BP event in**
2 **foraminifer isotope records from the Indus River delta in the Arabian Sea**

3
4 Alena Giesche¹, Michael Staubwasser², Cameron A. Petrie³, and David A. Hodell¹

5
6 ¹ *Godwin Laboratory for Palaeoclimate Research, Department of Earth Sciences, University of*
7 *Cambridge, Cambridge, CB2 3EQ, United Kingdom*

8 ² *Institute for Geology und Mineralogy, University of Cologne, Zùlpicher Str. 49a, 50674 Cologne,*
9 *Germany*

10 ³ *Department of Archaeology, University of Cambridge, Cambridge, CB2 3DZ, United Kingdom*

11
12 *Correspondence to: Alena Giesche (ag927@cam.ac.uk)*

13
14
15
16
17
18
19
20
21
22
23
24
25
26
27
28
29
30
31
32
33
34
35
36
37
38
39
40
41
42
43
44
45
46
47
48
49
50
51

52 **Abstract**

53
54 The plains of northwest South Asia receive rainfall during both the Indian Summer (June-September)
55 and Winter (December-March) Monsoon. Researchers have long attempted to deconstruct the
56 influence of ~~both these~~ precipitation regimes in paleoclimate records, in order to better understand
57 regional climatic drivers and their potential impact on human populations. The Mid-Late Holocene
58 transition between 5.3-3.3 ka BP is of particular interest in this region because it spans the period of
59 the Indus Civilization from its early development, ~~through its urbanization and on-~~to eventual
60 transformation ~~into a rural society~~. ~~The An~~ oxygen isotope record of the surface-dwelling planktonic
61 foraminifer *Globigerinoides ruber* from the northeast Arabian Sea provided evidence for an abrupt
62 decrease in rainfall and reduction in Indus River discharge at 4.2 ka BP, which the authors linked to
63 the decline of the urban phase of the Indus Civilization (Staubwasser et al., 2003). Given the
64 importance of this study, we used the same core (63KA) to ~~replicate the oxygen isotope profiles of a~~
65 ~~larger size fraction of G. ruber than measured previously and, in addition, we measured~~ measure the
66 oxygen isotope profiles of two other foraminifer species at decadal resolution over the interval from
67 5.4 to 3.0 ka BP, ~~and replicate a larger size fraction of G. ruber than measured previously~~. By selecting
68 both thermocline-dwelling (*Neogloboquadrina dutertrei*) and shallow-dwelling (*Globigerinoides*
69 *sacculifer*) species, we provide enhanced detail of the climatic changes that occurred over this crucial
70 time interval. We found evidence for a period of increased surface water mixing, which we suggest
71 was related to a strengthened winter monsoon with a peak intensity over 200 years from 4.5 to 4.3
72 ka BP. The time of greatest change occurred at 4.1 ka BP when both the summer and winter monsoon
73 weakened, resulting in a reduction in rainfall in the Indus region. The earliest phase of the urban
74 Mature Harappan period coincided with the period of inferred stronger winter monsoon between 4.5-
75 4.3 ka BP, whereas the end of the urbanized phase ~~followed~~ occurred some time after the decrease
76 in both the summer and winter monsoon strength by 4.1 ka BP. Our findings provide evidence that
77 the initial growth of large Indus urban centers ~~was coincident~~ coincided with increased winter rainfall,
78 whereas the contraction of urbanism and change in subsistence strategies followed a reduction in
79 rainfall of both seasons.

80
81
82
83
84
85
86
87
88
89
90
91
92
93
94
95
96
97
98
99
100

101
102
103
104
105
106
107
108
109
110
111
112
113
114
115
116
117
118
119
120
121
122
123
124
125
126
127
128
129
130
131
132
133
134
135
136
137
138
139
140
141
142
143
144
145
146
147

1. Introduction

The ~4.2 ka BP event is considered to be a defining event of the Mid-Late Holocene transition period (Mayewski et al., 2004), and is marked by intense aridity in much of western Asia, which has been linked to cultural transitions in Mesopotamia, Egypt, and the Indus Civilization (Staubwasser and Weiss, 2006; Weiss, 2016). Recently, a climate reconstruction from Mawmluh cave in northeastern India has been used to formally demarcate the post-4.2 ka BP time as the Meghalayan Age (Letter from the 44th International Union of Geological Sciences, 2018; Walker et al., 2012). However, defining the exact timing and extent of aridity at ~4.2 ka BP remains an open question (Finné et al., 2011; Wanner et al., 2008). In this special issue devoted to the “4.2 ka event”, we provide new paleoclimate data from a marine core in the northern Arabian Sea over this critical time interval to better understand the changes that occurred in both winter and summer hydroclimate over the Indian Subcontinent.

The $\delta^{18}\text{O}$ record of *Globigerinoides ruber* from marine core 63KA, obtained from the Arabian Sea off the coast of Pakistan and produced by Staubwasser et al. (2003), was among the first well-resolved paleoclimate records to suggest a link between a decrease in Indus River discharge around 4.2 ka BP and the decline of the urban phase of the Indus Civilization. Since the publication of this record, several other terrestrial paleoclimate reconstructions from the region (Berkelhammer et al., 2012; Dixit et al., 2014, 2018; Giosan et al., 2012; Kathayat et al., 2017; Menzel et al., 2014; Nakamura et al., 2016; Prasad and Enzel, 2006), and a number of marine reconstructions (Giosan et al., 2018, ~~in review~~; Gupta et al., 2003; Ponton et al., 2012) have added to our understanding of the complex relationship between the Indus Civilization and climate change. New questions have also emerged about the relative importance of winter rain from the Indian Winter Monsoon (IWM) system and summer rain from the Indian Summer Monsoon (ISM) during the critical time period from 5.4 to 3.0 ka BP, which spans the pre-urban, urban, and post-urban phases of the Indus Civilization (Giosan et al., 2018, ~~in review~~; Petrie et al., 2017; Prasad and Enzel, 2006). This is because the winter rain zone partially overlaps with the summer rain zone (Figure 1), and provides a critical supply of rain and snowfall for the Indus River basin. However, we currently understand much less about the behavior of the IWM than the ISM.

At its height, the Indus Civilization spanned a considerable geographical area with a greater extent than ~~all~~ the other ancient civilizations of its time (Agrawal, 2007; Possehl, 2003; ~~Wheeler, 1968~~). Today, the region that was once occupied by Indus populations is marked by a heterogeneous rainfall pattern, and some sites-locations in the central Thar desert receive as little as 100 mm yr⁻¹, which is only about 10% of the amount of direct annual rainfall ~~seen in the northeastern region close~~ compared to New Delhi. Scarce direct precipitation in the central regions around the Thar Desert is supplemented in some cases by fluvial or groundwater sources. In addition, the distribution of winter rain (increasing towards the northwest) is distinct from summer rain (increasing towards the east), making regions variably suitable for growing certain crops and grazing (Petrie et al., 2017; Petrie and Bates, 2017). While many paleoclimate studies from South Asia (references A-C, I, K-M, S, and U in Figure 1) have theorized about the overall climatic impact of drought (and in most cases identified summer monsoon as the cause), it is important to identify changes in the relative

148 contributions and timing of seasonal rainfall from both the winter and summer monsoons.
149 Previously, it has not been possible to reliably differentiate winter and summer rain in
150 reconstructions from the Indus region.

151

152 In this study, we re-examined the same marine core (63KA) used in the original [research of](#)
153 Staubwasser et al. (2003) ~~paper~~. We first assessed the reproducibility of the *Globigerinoides*
154 *ruber* $\delta^{18}\text{O}$ record using a larger size fraction of the same species for the time period 5.4-3.0
155 ka BP. We also measured the $\delta^{18}\text{O}$ of two additional foraminifer species, *G. sacculifer*
156 (*Globigerinoides sacculifer*) and *N. dutertrei* (*Neogloboquadrina dutertrei*), which live deeper
157 than *G. ruber* in the water column. The different ecologies of these ~~two~~ three species provide
158 additional information with which to evaluate the multiple $\delta^{18}\text{O}$ records and assess seasonal
159 changes in the paleoceanography of the northeastern Arabian Sea near the mouth of the
160 Indus River.

161

162 The $\delta^{18}\text{O}$ of foraminifera has been widely applied as an indicator of temperature and salinity
163 changes (Duplessy et al., 1992; Maslin et al., 1995; Wang et al., 1995; Rohling, 2000; [among](#)
164 [others](#)). Measuring the $\delta^{18}\text{O}$ of species calcifying at different depths can provide further
165 information about upper ocean seasonal hydrography such as surface water mixing, depth of
166 the thermocline, and upwelling (Ravelo and Shackleton, 1995). ~~Such~~ Similar methods have
167 been applied by several other studies (Billups et al., 1999; Cannariato and Ravelo, 1997;
168 Norris, 1998; Steinke et al., 2010; Steph et al., 2009; among others), including a reconstruction
169 of East Asian Winter Monsoon strength in the South China Sea (Tian et al., 2005). ~~We~~ Here
170 we ~~applied~~ a ~~similar-comparable~~ method to samples from core 63KA in the northeastern
171 Arabian Sea because surface waters at this location are influenced by freshwater discharge
172 from the Indus River and direct precipitation during the summer monsoon months, whereas
173 enhanced upper ocean mixing occurs during the winter monsoon. We hypothesized that our
174 new measurements of $\delta^{18}\text{O}$ of *G. sacculifer* and *N. dutertrei* would allow us to track changes
175 in upper ocean mixing. Weaker IWM winds are expected to result in a shorter duration and/or
176 less intense upper ocean mixing, although how this signal is ultimately related to the amount
177 or distribution of winter rainfall in the Indus River catchment has not been demonstrated
178 conclusively. Dimri (2006) studied Western Disturbances for the time period 1958-1997, and
179 noted that surplus years of surplus winter precipitation are linked to significant heat loss over
180 the northern Arabian Sea, which is mainly attributed to intensified westerly moisture flow
181 and enhanced evaporation. Such conditions would promote deeper winter mixing, and
182 provide a basis for relating thermocline depth with IWM intensity. By comparing the $\delta^{18}\text{O}$ of
183 multiple species of foraminifera we seek to infer variations in the relative strengths of the
184 summer and winter monsoons, and by comparing the 63KA record to other nearby marine
185 and terrestrial records we evaluate the potential role that climate played in cultural
186 transformation of the Indus Civilization.

187

188 2. Site Description

189

190 2.1 Monsoon – land-based processes

191

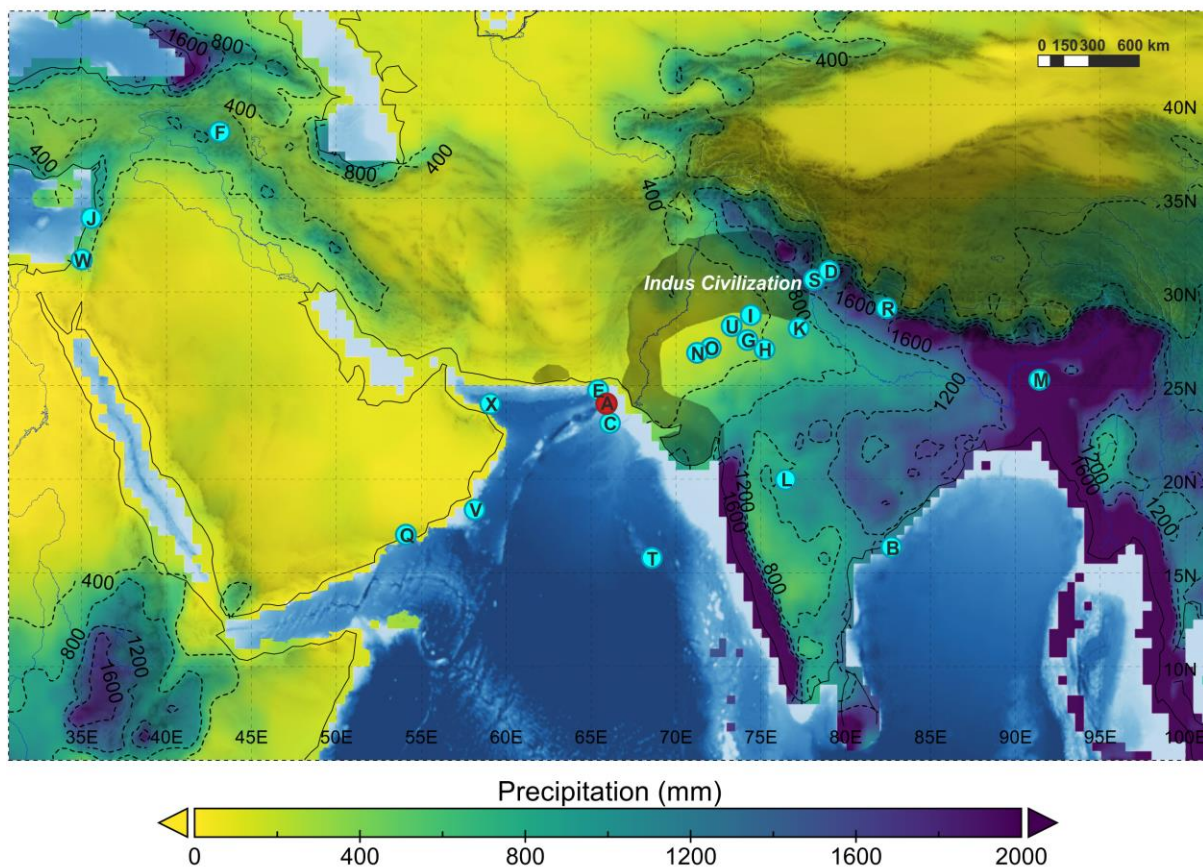
192 Today, most of the annual precipitation over northwest South Asia stems from the ISM, and
193 occurs mainly between June and September. The pressure gradient between the low-
194 pressure Tibetan Plateau and high-pressure Indian Ocean is accompanied by the ITCZ

195 (Intertropical Convergence Zone) reaching its northward maximum in summer, which draws
196 in moisture over the subcontinent via southwesterly winds from the Indian Ocean ([Fleitmann
197 et al., 2007](#); Gadgil, 2003). The summer rainfall gradient increases from the central Thar
198 Desert (as little as 100 mm direct summer rainfall per year) to the Himalaya mountains in the
199 north (>1000 mm) and the Aravalli range to the west (>500 mm) (Figure 1b).

200
201 The IWM rain falls between December through March, and is mainly the result of atmospheric
202 Western Disturbances (Dimri and Dash, 2012; Yadav et al., 2012) originating over the
203 Mediterranean and Black Sea (Hatwar et al., 2005) that allow for moisture incursion from the
204 Arabian Sea (Rangachary and Bandyopadhyay, 1987). During the IWM, the pressure gradient
205 is reversed from the summer condition, allowing the passage of Western Disturbances when
206 the ITCZ moves southward. As winter transitions to spring, predominantly northeasterly
207 winds shift to westerly winds (Sirocko, 1991) that result in peak winter rainfall over the plains
208 of northwest India in February and March. [Anomalously cool, evaporative conditions over the
209 northern Arabian Sea \(promoting deeper winter mixing\) also correlates with increased winter
210 precipitation in the western Himalayas \(Dimri, 2006\)](#). The winter rainfall gradient increases
211 from the southern Thar Desert (<10 mm per year) up to the Himalayas in the northwest (>400
212 mm) (Figure 1c). Overall, the IWM contributes between roughly 10 to 50% of the total annual
213 rainfall of northwest South Asia today.

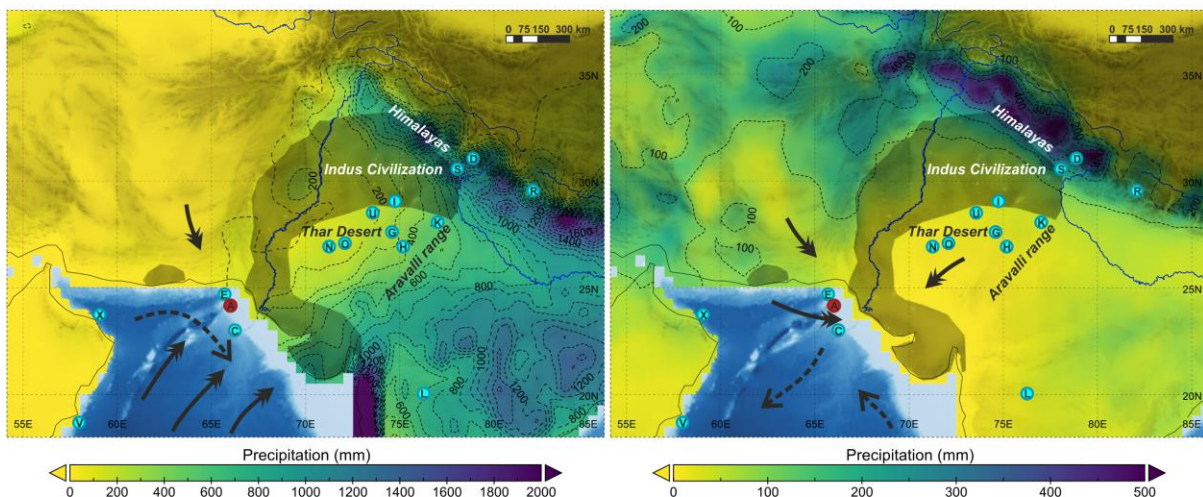
214

(a) Longterm mean (1981-2010) annual precipitation



(b) Longterm mean (1981-2010) summer precipitation

(c) Longterm mean (1981-2010) winter precipitation



215
216
217
218
219
220
221
222

Figure 1. a. Annual **b.** ISM (JJAS) **c.** IWM (DJFM) mean precipitation (1981-2010) isohyets taken from the GPCP V7 global gridded dataset ($0.5^\circ \times 0.5^\circ$ resolution) (Schneider et al., 2015); note the difference in scale for summer and winter precipitation (0-2000 mm vs. 0-500 mm). Rainfall data overlain on GEBCO 2014 ocean bathymetry dataset (Weatherall et al., 2015), and shaded region shows extent of the Indus Civilization. Bold arrows show main wind directions, dashed arrows show ocean surface currents. Other studies discussed in this paper indicated by letters:

- | | |
|---|---|
| A Core 63KA – (this study; Staubwasser et al., 2003) | E Core 39KG and 56KA – (Dose-Rolinski et al., 2001) |
| B Core 16A – (Ponton et al., 2012) | F Lake Van record – (Wick et al., 2003; Lemcke and Sturm, 1997) |
| C Core Indus 11C – (Giosan et al., 2018, <i>in review</i>) | G Didwana playa lake – (Singh et al., 1990) |
| D Din Gad peat record – (Phadtare, 2000) | |

- H Sambhar playa lake – (Sinha et al., 2006)
 I Karsandi playa lake – (Dixit et al., 2018)
 J Jeita cave speleothem – (Cheng et al., 2015)
 K Kotla Dahar lake – (Dixit et al., 2014)
 L Lonar lake – (Menzel et al., 2014)
 M Mawmluh cave speleothem – (Berkelhammer et al., 2012)
 N Kanod playa lake – (Deotare et al., 2004)
 O Bap Malar playa lake – (Deotare et al., 2004)
 Q Qunf cave speleothem – (Fleitmann et al., 2003)
 R Rara lake – (Nakamura et al., 2016)
 S Sahiya cave speleothem – (Kathayat et al., 2017)
 T Foraminifer trap EAST – (Curry et al., 1992)
 U Lunkaransar playa lake – (Enzel et al., 1999)
 V Core 723A, RC27-14, RC27-23, RC27-28 – (Gupta et al., 2003), (Overpeck et al., 1996)
 W Soreq cave speleothem – (Bar-Matthews et al., 2003; Bar-Matthews and Ayalon, 2011)
 X Core M5-422 – (Cullen et al., 2000)

223

224 The Indus and the other rivers that make up Punjab are partly fed by winter snow and ice melt
 225 from their upper mountain catchment areas. Melting peaks during the summer months
 226 around July-August (Yu et al., 2013), which coincides with the peak of ISM rainfall, and Indus
 227 River discharge reaches its maximum during August (Karim ~~et al.,~~ [and Veizer, 2002](#)). The
 228 proportion of winter to summer precipitation contributing to the Indus River is not entirely
 229 clear, although one study has estimated a 64-72% contribution of winter precipitation from
 230 the deuterium excess of Indus River water (Karim ~~et al.,~~ [and Veizer, 2002](#)), whereas a previous
 231 study estimated a lower 15-44% contribution of snowmelt to Indus tributaries (Ramasastrri,
 232 1999). Since the 1960s, the Indus River has seen ~~a~~ more than a 50% reduction in discharge
 233 because of the construction of barrages as well as the diversion of water for agricultural uses
 234 (Ahmad et al., 2001).

235

236 2.2 Hydrography – [core site and ocean-based processes](#)

237

238 Core 63KA was obtained by the PAKOMIN cruise in 1993 (von Rad et al., 1995). The laminated
 239 core from the northeastern Arabian Sea (24° 37' N, 65° 59' E) was taken at 316 m water depth
 240 on the continental shelf, ~100 km west of the Indus River delta. The core has high
 241 sedimentation rates (equivalent to a temporal resolution of around 18 years/cm in the period
 242 of interest, 5.4-3.0 ka BP), and all foraminifer proxies were produced from the same laminated
 243 core with no bioturbation. An important aspect of core 63KA is that different components of
 244 the monsoon system are co-registered in the same sediment core, thereby permitting an
 245 explicit evaluation of the relative timing of different parts of the climate system (e.g., ISM and
 246 IWM).

247

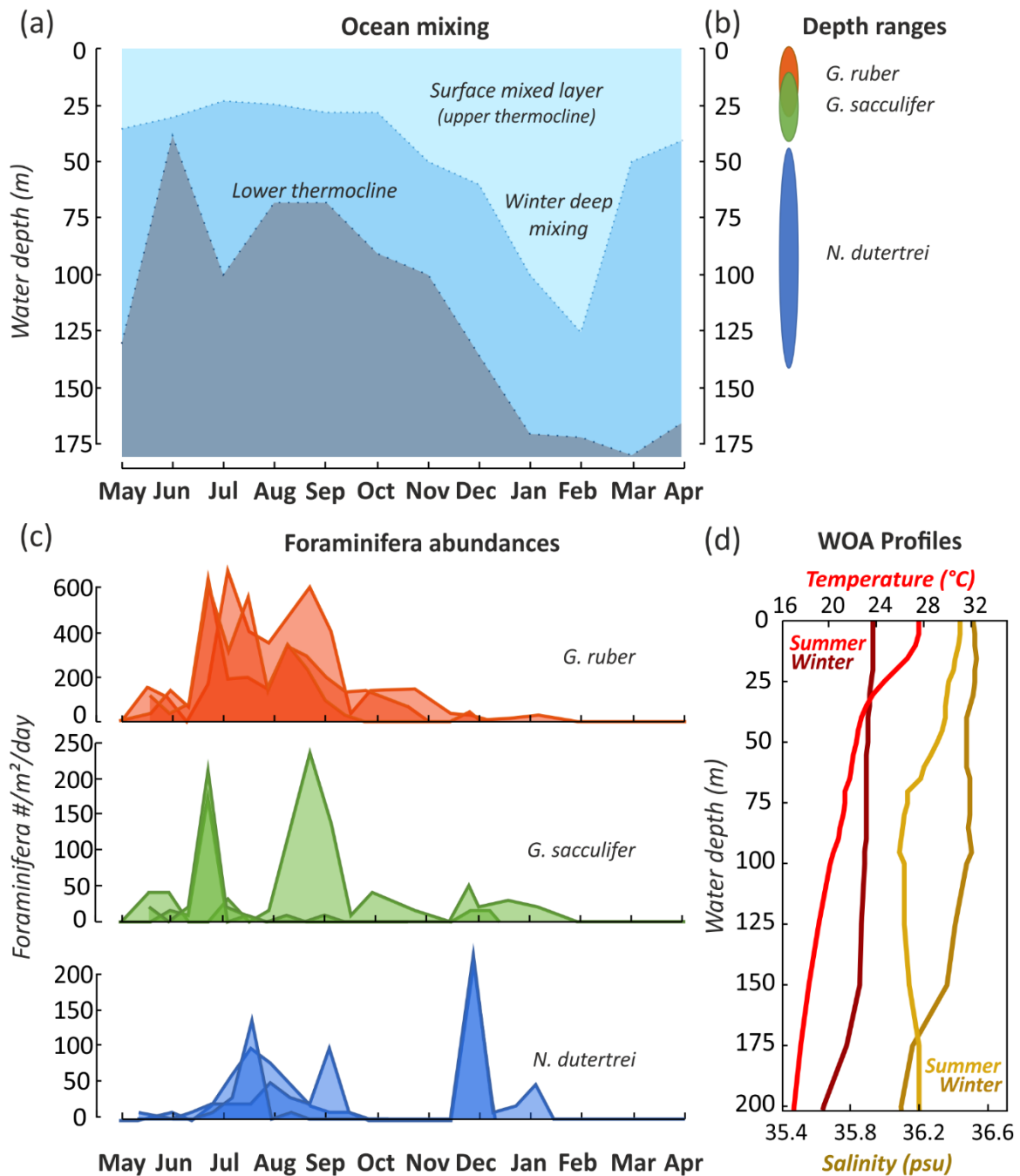
248 Modern hydrographic conditions in the northeastern Arabian Sea are highly influenced by the
 249 seasonal monsoon. During summertime, highest sea surface temperatures (SSTs) are
 250 observed along with a shallow mixed layer depth <25 m (Schulz et al., 2002) (Figure 2a). A low
 251 salinity plume surrounds the Indus River delta and shoreline extending as far as the coring
 252 location (Supplemental Figure S1). The reverse occurs in winter when the lowest SSTs are
 253 accompanied by surface water mixing to >125 m, resulting in warming of the deeper waters
 254 (Schulz et al., 2002). [Northeasterly winds promote convection in the northeastern Arabian](#)
 255 [Sea by cooling and evaporation of surface water \(Banse, 1984; Madhupratap et al., 1996\),](#)
 256 [and during the transition from winter to spring, wind directions shift from northeasterly to](#)
 257 [westerly \(Sirocko, 1991\), promoting a period of upwelling in the northeastern Arabian Sea](#)
 258 [\(Staubwasser et al., 2002; Rao, 1981\).](#)

259

260 The northern Arabian Sea is dominated by highly saline (up to 37 psu) surface waters ~~of~~
 261 [the known as](#) Arabian Sea High Salinity Water ~~Mass~~ (ASHSW), which extends s from the surface

262 ~~down~~ to 100 m depth (Joseph and Freeland, 2005). ~~The~~is high salinity ~~can be~~is explained
263 by the high evaporative rates over this region. ASHSW forms in the winter, but is prevented
264 from reaching our coring site on the shelf by northerly subsurface currents until the summer
265 (Kumar and Prasad, 1999). Along coastal areas, the ASHSW is starkly contrasted by the fresh
266 water discharge of the Indus River, combined with direct precipitation. In contrast, surface
267 waters in the Bay of Bengal on the eastern side of India have much lower surface water
268 salinity, because of overall higher precipitation and stronger stratification from weaker winds
269 (Shenoi et al., 2002). The heightened evaporative conditions and highly saline surface waters
270 of the northeastern Arabian Sea make it a sensitive study location to observe changes in
271 discharge of the entire Indus River catchment area – ultimately tracking changes in monsoon
272 strength. Unlike individual terrestrial records, which may be affected by local climatic
273 processes, the marine record from core 63KA is more likely to integrate regional changes of
274 the large-scale ocean-atmosphere system.

275
276 Planktonic foraminifera complete their life cycle within a few weeks (Bé and Hutson, 1977).
277 Peak abundances indicate the time of year when each species tends to calcify, thereby
278 recording the $\delta^{18}\text{O}$ and temperature of the seawater in their CaCO_3 shells primarily during
279 certain seasons. Foraminifer abundances in the eastern Arabian Sea have been studied by
280 Curry et al. (1992) using sediment traps deployed at shallow (~1400 m) and deep (~2800 m)
281 water depths (“T” in Figure 1a). ~~Peak abundances for~~ *G. ruber* and *G. sacculifer* ~~occur~~ have
282 peak abundances during the summer months (June-September), whereas *N. dutertrei* ~~peak~~
283 lives mainly during the winter ~~as well as~~ and has a secondary peak in ~~with a secondary peak~~
284 in summer months (Figure 2c). Preferred depth ranges for each species reflect their ecological
285 niches, including requirements for nutrients and tolerance for ranges of temperature and
286 salinity (Bé and Hutson, 1977; Hemleben et al., 2012). *G. ruber* lives in the upper surface
287 waters (0-10 m), *G. sacculifer* is found in slightly deeper surface waters (10-40 m), and *N.*
288 *dutertrei* inhabits the base of the mixed layer near the thermocline (40-140 m) (estimates
289 based on ranges from Farmer et al. (2007) and the local CTD profiles) (Figure 2d).
290



291
 292 **Figure 2.** a. Seasonal surface water mixing depth based on station EPT-2 located nearby the coring site
 293 of 63KA (adapted from Schulz et al., 2002 who also used data from Hastenrath and Lamb, 1979) b.
 294 Foraminifer depth ranges based on CTD profile c. Foraminifer abundances from EAST traps
 295 (overlapping peaks indicate data from multiple traps): *G. ruber* (orange), *G. sacculifer* (green), and *N.*
 296 *dutertrei* (blue) (adapted from Curry et al., 1992 using Zaric, 2005) d. CTD-World Ocean Atlas (WOA)
 297 mean (1955-2012) temperature (red) and salinity (yellow) profiles at 24.875°N, 65.875°E from
 298 station 11 at coring location, shown for summer (JAS) and winter (JFM) seasons (Locarnini et al., 2013;
 299 Zweng et al., 2013) taken September 1993 (von Rad, 2013).

300

301 3. Materials and Methods

302

303 3.1 Age model

304

305 The radiocarbon dates from Staubwasser et al. (2002, 2003) were obtained from 80 samples
306 of mainly the foraminifer *G. sacculifer* and three samples of *O. universa*. In the interval of
307 interest (5.4-3.0 ka BP), there are 15 radiocarbon dates with a 95% confidence range of 30-
308 130 years. The average sample resolution is 18 years/cm. Bayesian age modelling software,
309 BACON v2.3.3 (Blaauw and Christen, 2011), was used as an R-package to update the age
310 model of core 63KA. No major difference exists between the old and new age models, except
311 for the period 13-11 ka BP (Supplemental Figure S5, Table S2). IntCal13 was used for
312 radiocarbon calibration (Reimer et al., 2013) with marine reservoir ages provided by
313 Staubwasser et al. (2002, 2003).

314

315 3.2 Stable isotope analysis

316

317 Oxygen and carbon isotopes were measured on three species of foraminifera selected from
318 washed samples at 1-cm intervals throughout 132 cm of the core covering 5.4-3.0 ka BP: *G.*
319 *ruber* (white, *sensu stricto*), *G. sacculifer*, and *N. dutertrei*. For *G. ruber*, 12 ± 8 foraminifera
320 were picked from the 400-500µm size fraction with an average weight of 21.4 ± 2.5µg. The
321 400-500µm size fraction was picked because too few specimens remained in the size fraction
322 315-400µm used by Staubwasser et al. (2003). For *G. sacculifer*, 34 ± 7 foraminifera were
323 picked from the 315-400µm size fraction with an average weight of 21.9 ± 2.6µg. For *N.*
324 *dutertrei*, 34 ± 4 foraminifera were picked from the 315-400µm size fraction with an average
325 weight of 25.9 ± 2.2µg. At some depth levels in the core there were insufficient foraminifera
326 for measurement, along with outlier measurements in two cases, leaving 11-14 gaps in the *G.*
327 *ruber* 400-500µm record, 3-4 gaps in the *G. sacculifer* record, and no gaps for *N. dutertrei*. The
328 published *G. ruber* is from the 315-400µm size fraction and contains 17 gaps in the depth
329 range examined (Staubwasser et al., 2003).

330

331 All foraminifera were weighed, crushed, and dried at 50° C. Samples were cleaned for 30
332 minutes with 3% H₂O₂, followed by a few drops of acetone, ultrasonication, and drying
333 overnight. –Where sample weights exceeded 80µg, oxygen and carbon isotopes were
334 measured using a Micromass Multicarb Sample Preparation System attached to a VG SIRA
335 Mass Spectrometer. In cases of smaller sample sizes, the Thermo Scientific Kiel device
336 attached to a Thermo Scientific MAT253 Mass Spectrometer was used in dual inlet mode. This
337 method adds 100% H₃PO₄ to the CaCO₃, water is removed cryogenically, and the dry CO₂ is
338 analyzed isotopically by comparison with a laboratory reference gas. For both measurement
339 methods, 10 reference carbonates and 2 control samples were included with every 30
340 samples. Results are reported relative to VPDB, and internal precision/long-term
341 reproducibility of laboratory standards (e.g., Carrara marble) is better than ±0.08‰ for δ¹⁸O
342 and ±0.06‰ for δ¹³C. External precisions/Reproducibility of foraminiferal measurements were
343 was estimated by five triplicate (three separately picked) measurements of *G. ruber* (400-
344 500µm) that yielded one standard deviation of ±0.12‰ (δ¹⁸O) and ±0.10‰ (δ¹³C). For *G.*
345 *sacculifer* (315-400µm) the standard deviation of eight triplicate measurements were/was
346 ±0.07‰ (δ¹⁸O) and ±0.07‰ (δ¹³C), and for *N. dutertrei* (315-400µm) the standard deviation
347 of nine triplicate measurements was ±0.06‰ (δ¹⁸O) and ±0.07‰ (δ¹³C).

348

349 To calculate equilibrium values of δ¹⁸O_{calcite(PDB)}, we used the CTD profile from station 11
350 (24.62° N, 66.07° E) (Figure 2d) taken in September 1993 during PAKOMIN *Sonne* cruise no.
351 90 (von Rad, 2013), which is nearly identical to the location of core 63KA (24.62° N 65.98° E).

352 The $\delta^{18}\text{O}_{\text{water(SMOW)}}$ was calculated from salinity following Dahl and Oppo (2006), and
353 $\delta^{18}\text{O}_{\text{calcite(SMOW)}}$ was further calculated using the calcite-water equation of Kim and O’Neil
354 (1997). We also used the equation of Shackleton (1974) as a comparative method for
355 calculating $\delta^{18}\text{O}_{\text{calcite(PDB)}}$.

356

357 3.3 Statistical treatment

358

359

360 Statistical tests were applied to the raw data from the $\delta^{18}\text{O}$ and $\delta^{13}\text{C}$ time series, including the
361 package SiZer (Chaudhuri and Marron, 1999; Sonderegger et al., 2009) in R software (2016)
362 that calculates whether the derivative of a time series exhibits significant changes given a
363 range of timespans. A Pearson’s correlation test (confidence level 95%) was done on paired
364 samples from both size fractions of *G. ruber*. We also conducted a Welch’s t-test to determine
365 if the mean population of $\delta^{18}\text{O}$ is significantly different before and after 4.1 ka BP. ~~We applied~~
366 ~~a range of smoothing windows (bandwidth of 20–500 years) to assess the significance of~~
367 ~~changes in the isotope records throughout the time series.~~

368

369 As in the original data of Staubwasser et al. (2003), the oxygen isotope results show great
370 variability and distinguishing long-term trends in these data requires benefits from statistical
371 smoothing for visualization purposes. ~~To reduce the variance in the data and identify~~
372 ~~trends.~~ After completing all statistical tests and performing the differences on the raw data
373 (132 depths), the $\delta^{18}\text{O}$ and $\delta^{13}\text{C}$ data from 5.4–3.0 ka BP were first resampled to constant 1-
374 year intervals using linear interpolation. ~~A~~ loess (locally weighted) smoothing function was
375 ~~then~~ applied to the $\delta^{18}\text{O}$ and $\delta^{13}\text{C}$ data from 5.4–3.0 ka BP data, using a 210-year moving
376 window as described by Staubwasser et al. (2003). Loess smoothing uses weighted least
377 squares, which places more importance on the data points closest to the center of the
378 smoothing interval. The bandwidth of 210 years was considered an optimal-reasonable time
379 window for capturing the overall trends in the dataset (other time windows are shown for
380 comparison in Supplemental Figure S2).

381

382 ~~Where step changes occur in $\delta^{18}\text{O}$ we also conducted a Student’s t test to determine if the~~
383 ~~mean population of $\delta^{18}\text{O}$ is significantly different before and after the change.~~

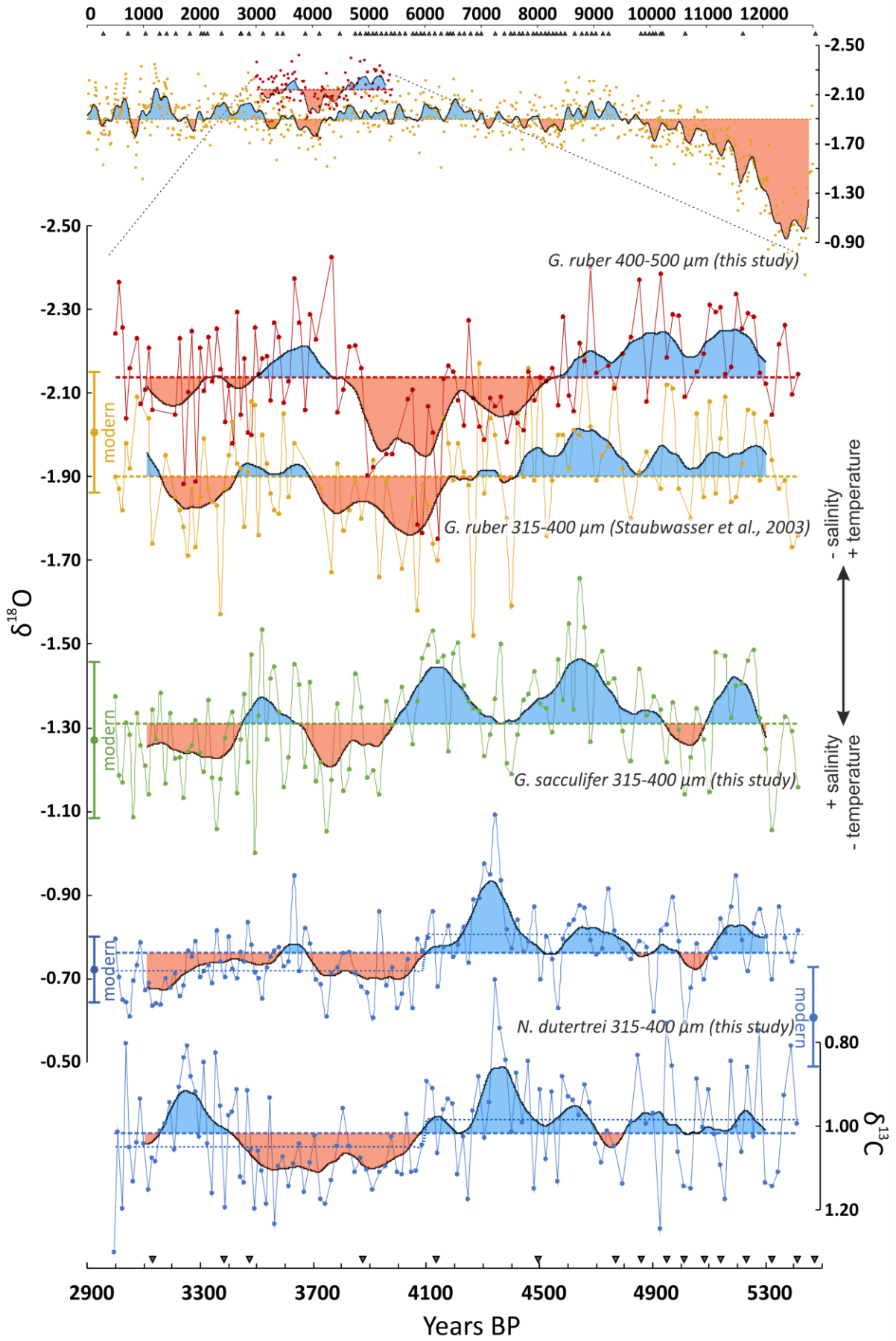
384

385 4. Results

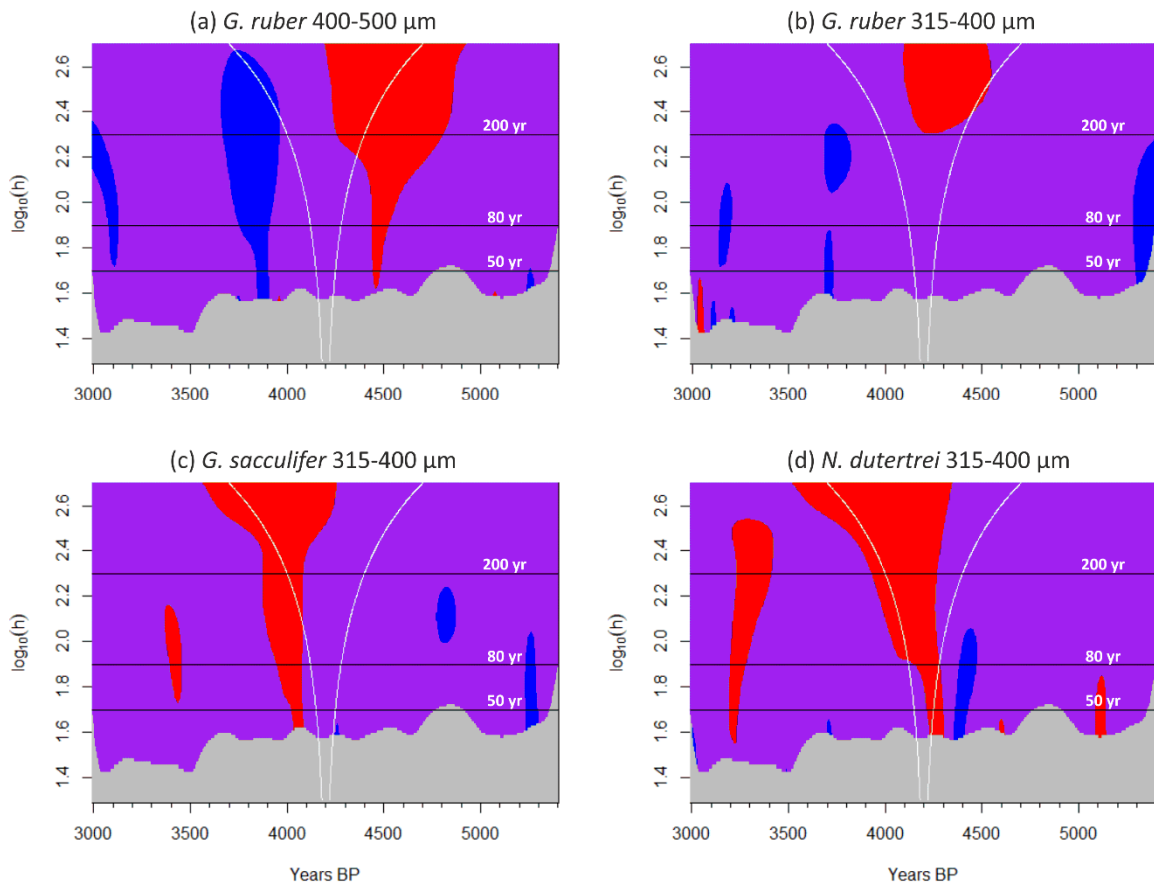
386

387 The new $\delta^{18}\text{O}$ measurements of *G. ruber* (400–500 μm) parallel the published record of *G.*
388 *ruber* (315–400 μm) (Staubwasser et al., 2003), but the $\delta^{18}\text{O}$ of the specimens from the larger
389 size fraction is offset by -0.23‰ on average (Figure 3). The two records from two size
390 fractions, produced in different laboratories by different investigators, display a weak positive
391 correlation for the raw data ($R = 0.25$, $p < 0.01$, $n = 109$, slope 0.2726, intercept -1.3336), and
392 the 210-year smoothed records reveal good agreement in the overall trends of the data and
393 a strong correlation for the 210-year smoothed records ($R = 0.7$, slope 0.53, intercept -0.77).
394 When comparing the two *G. ruber* records, it is apparent that the increasing trend in $\delta^{18}\text{O}$
395 starts well before ~4.2 ka BP – perhaps as early as ~4.9 ka BP. This trend is also observed with
396 the SiZer analysis, which identifies a significant increase in $\delta^{18}\text{O}$ anywhere from 4.9 to 4.2 ka
397 BP depending on which smoothing window is selected (Figure 4). The new $\delta^{18}\text{O}$ record of *G.*
398 *ruber* (400–500 μm) shows additional detail after the ~4.2 ka BP event – i.e. specifically, a

399 double-peak maximum occurring at 4.1 and 3.95 ka BP that is related to seven discrete
400 measurements with high $\delta^{18}\text{O}$ values. These maxima are offset from the average $\delta^{18}\text{O}$ value
401 by +0.18‰ (smoothed average), or up to +0.38‰ when considering the maximum individual
402 measurement at 4.1 ka BP. The offsets from the average values exceed one standard
403 deviation of the entire record from 5.4-3.0 ka BP, which is 0.13‰. Although *G. ruber* shows
404 an event at 4.1 ka BP, it does not show a permanent step change: A Student's-Welch's t-test
405 comparing the means of pre- and post-4.1 ka BP indicates that the +0.07‰ shift in mean $\delta^{18}\text{O}$
406 values of *G. ruber* (315-400 μm) is statistically significant (t value = 2.9, $p < 0.01$, $n = 115$), ~~and~~
407 but the +0.0403‰ shift in mean $\delta^{18}\text{O}$ values of *G. ruber* (400-500 μm) is weakly-not significant
408 (t value = 1.75, $p < 0.12$, $n = 118$).
409



411 **Figure 3.** Core 63KA $\delta^{18}\text{O}$ *G. ruber* from two size fractions: 400-500 μm (red) (this study), 315-400 μm
 412 (orange) (Staubwasser et al., 2003), shown in the context of the original record and also zoomed in
 413 over 5.4-3.0 ka BP. $\delta^{18}\text{O}$ of *G. sacculifer* 315-400 μm (green), and $\delta^{18}\text{O}$ and $\delta^{13}\text{C}$ of *N. dutertrei* 315-
 414 400 μm (blue) are shown over the interval 5.4-3.0 ka BP. Data are shown with a 210-year loess
 415 smoothing, and modern surface values $\pm 1\sigma$ are plotted for comparison and $\pm 1\sigma$ error bars. Mean
 416 values for all species are denoted by the dotted line, and the pre- and post-4.1 ka BP mean values are
 417 indicated by an additional dotted line for *N. dutertrei*. Individual AMS radiocarbon dates are denoted
 418 by triangles near the timeline.
 419



420 **Figure 4.** SiZer 1st derivative analysis (Chaudhuri and Marron, 1999; Sonderegger et al., 2009) applied
 421 to $\delta^{18}\text{O}$ of a. *G. ruber* 400-500 μm , b. *G. ruber* 315-400 μm , c. *G. sacculifer* 315-400 μm , d. *N. dutertrei*
 422 315-400 μm . The red areas indicate statistically significant increases in $\delta^{18}\text{O}$, the blue represent
 423 decreases, and the purple no significant change. Black horizontal lines are the smoothing bandwidths
 424 ($h = 50, 80,$ and 200 years). The distance between the white lines denotes the change in smoothing
 425 bandwidth scaled to the x-axis.
 426

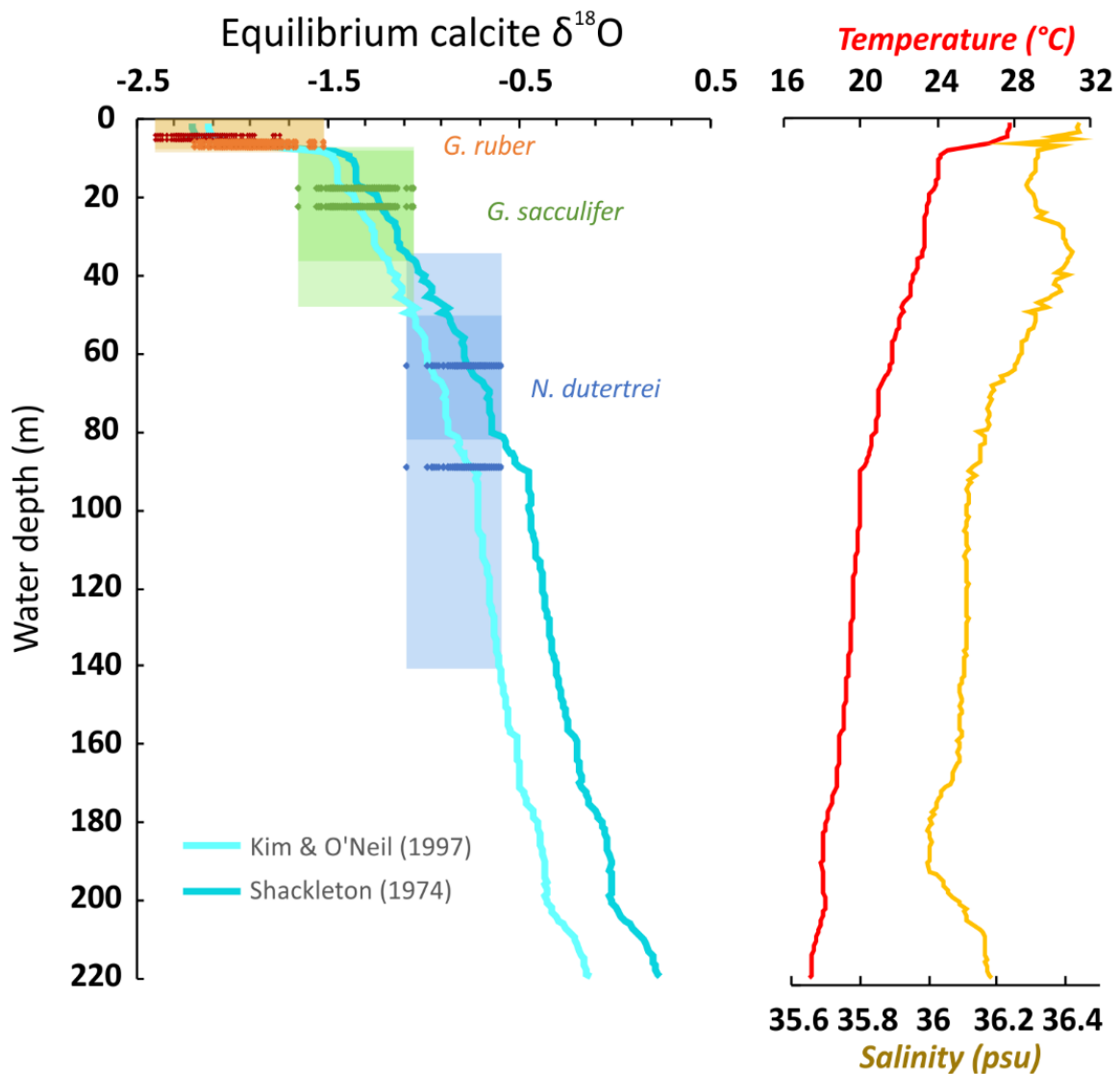
427
 428 The relative differences in $\delta^{18}\text{O}$ of the planktonic species studied (*G. ruber*, *G. sacculifer* and
 429 *N. dutertrei*) reflect the temperature and salinity of their habitat in the water column: $\delta^{18}\text{O}$
 430 *G. ruber* < $\delta^{18}\text{O}$ *G. sacculifer* < $\delta^{18}\text{O}$ *N. dutertrei* (Figure 35). *G. sacculifer* is offset from *G. ruber*
 431 (315-400 μm) by approximately +0.57‰, whereas *N. dutertrei* is offset by +1.14‰. The larger
 432 size fraction of *G. ruber* (400-500 μm) is offset from *G. ruber* (315-400 μm) by -0.23‰. The
 433 offsets among species are maintained throughout the entire record (Figure 35). We also
 434 measured $\delta^{18}\text{O}$ values near the top of the core (approximately the last 200 years) for all three
 435 species in the 315-400 μm size fraction, which continue to show the same offsets

436 (Supplemental Figure S3). The $\delta^{18}\text{O}$ of *G. ruber* shows the greatest variance and *N. dutertrei*
 437 shows the least (Supplemental Figure S4, Table S1).

438

439 Equilibrium calcite calculations based on the salinity and temperature measurements from
 440 the September 1993 CTD profile of station 11 of the PAKOMIN Cruise (von Rad, 2013) show
 441 the expected depth habitats of the three foraminifer species (Figure 65). *G. ruber* is generally
 442 found at 0-30 m, *G. sacculifer* at 15-40 m, and *N. dutertrei* at 60-150 m (Farmer et al., 2007).
 443 Using the CTD profile from our core location, we compare these depth ranges with the
 444 measured $\delta^{18}\text{O}$ values. The calculated depths ranges agree well with those expected on the
 445 basis of other studies, placing *G. ruber* in the upper 10 m, *G. sacculifer* 10-40 m, and *N.*
 446 *dutertrei* 40-140 m.

447



448

449 **Figure 65.** $\delta^{18}\text{O}$ of equilibrium calcite (left) calculated from the CTD temperature and salinity profile
 450 at station 11 (von Rad, 2013) (right) with projected depth ranges of *G. ruber* 400-500 μm (red), *G. ruber*
 451 315-400 μm (orange), *G. sacculifer* 315-400 μm (green), *N. dutertrei* 315-400 μm (blue). We show
 452 estimated values using both the original paleotemperature equation of Shackleton (1974) (dark teal),
 453 and Kim & O'Neil (1997) (turquoise). Horizontal ranges show the measured $\delta^{18}\text{O}$ values of each species
 454 between 5.4-3.0 ka BP.

455
456
457
458
459
460
461
462
463
464
465
466
467
468
469
470
471
472
473
474
475
476
477
478
479
480
481

~~The most obvious trend in the *G. sacculifer* $\delta^{18}\text{O}$ is the increase~~ around 4.1 ka BP. ~~A, and a Student's-Welch's~~ t-test comparing the means of pre- and post-4.1 ka BP indicates that the +0.0708‰ shift in mean $\delta^{18}\text{O}$ values is statistically significant (t value = 3.98, $p < 0.01$, $n = 128$). SiZer analysis also points to a statistically significant increase at ~4.1-3.9 ka BP, when considering all smoothing time windows between 20 and 500 years (Figure 44).

~~Likewise, the dominant trend change~~ in the $\delta^{18}\text{O}$ of *N. dutertrei* is a mean increase at 4.1 ka BP (Figure 37). SiZer analysis also identifies a significant decrease in $\delta^{18}\text{O}$ occurring mainly between 4.45 and 4.35 ka BP, followed by a significant increase between 4.3 and 4.1 ka BP (Figure 44). A ~~Student's-Welch's~~ t-test comparing the means of pre- and post-4.1 ka BP indicates that the +0.08‰ shift in mean $\delta^{18}\text{O}$ values is statistically significant (t value = 6.32, $p < 0.01$, $n = 132$), along with the +0.07‰ shift in mean $\delta^{13}\text{C}$ (t value = 3.3, $p < 0.01$, $n = 132$).

Differencing $\delta^{18}\text{O}$ of foraminifera (expressed as $\Delta\delta^{18}\text{O}$) in the same sample can ~~better sometimes improve the signal-to-noise ratio~~ emphasize signals of interest (Figure 68). The $\Delta\delta^{18}\text{O}$ of *G. ruber* 400-500 μm and *G. ruber* 315-400 μm size fractions shows increasing similarity between ~4.8 and 3.9 ka BP during the period of overall higher $\delta^{18}\text{O}$. The $\Delta\delta^{18}\text{O}$ of *N. dutertrei* and both size fractions of *G. ruber*, designated $\Delta\delta^{18}\text{O}_{d-r}$, reveals a period of more similar values between ~4.5 and 3.9 ka BP, with two minima at 4.3 and 4.1 ka BP. The $\Delta\delta^{18}\text{O}$ of *G. sacculifer* and both size fractions of *G. ruber* ($\Delta\delta^{18}\text{O}_{s-r}$) shows a period of similar values between 4.3 and 3.9 ka BP, with a minimum difference at 4.1 ka BP. In contrast, the $\Delta\delta^{18}\text{O}$ of *N. dutertrei* and *G. sacculifer* ($\Delta\delta^{18}\text{O}_{d-s}$) shows the most similarity between 4.5 and 4.2 ka BP with a minimum at 4.3 ka BP, followed by the maximum differences between 4.2 and 3.9 ka BP that peaks at 4.1 ka BP.

489 5. Discussion

490

491 5.1 Interpretation of foraminifer $\delta^{18}\text{O}$

492

493 The trends in the original $\delta^{18}\text{O}$ record of *G. ruber* (315-400 μm) by Staubwasser et al. (2003) is
494 confirmed-reflected by our independent $\delta^{18}\text{O}$ measurements of *G. ruber* in a larger size
495 fraction (400-500 μm), although an important difference exists suggesting a decrease in
496 freshwater discharge as early as 4.8 ka BP. The larger size fraction is offset by approximately
497 -0.2‰, which is similar to the size-related fractionation of -0.3‰ per +100 μm for *G. ruber*
498 reported by Cayre and Bassinot (1998), and could be attributed to size-related vital effects.
499 Alternatively, part of the offset might be explained by interlaboratory calibration considering
500 the data were produced using two different methods and mass spectrometers.

501

502 The observed 4.1 ka BP maximum in $\delta^{18}\text{O}$ of *G. ruber*, living near the surface during summer
503 months, could be attributed to either decreased SST or increased surface water salinity
504 (Bemis et al., 1998). Staubwasser et al. (2003) acknowledged that a decrease in SST could
505 cause the increase in $\delta^{18}\text{O}$ in the *G. ruber* record, but argued that this explanation is unlikely
506 because a *G. ruber* $\delta^{18}\text{O}$ record from core M5-422 in the northwestern Arabian Sea shows
507 opposing trends over the same time period (Cullen et al., 2000), and a local alkenone SST
508 proxy record shows relatively higher temperatures in the same period (Doose-Rolinski et al.,
509 2001). If the ~0.2‰ (relative to mean) increase in $\delta^{18}\text{O}$ of *G. ruber* at 4.1 ka BP was caused by
510 temperature change rather than salinity, a ~1° C cooling of surface water is implied would be
511 required (Kim and O'Neil, 1997).

512

513 Following Staubwasser et al. (2003), we interpret the $\delta^{18}\text{O}$ variations of *G. ruber* to be
514 predominantly a salinity signal. Salinity at the core site is dependent on changes in Indus River
515 discharge, local run-off, and direct precipitation. Although the ISM would be the main
516 influence on direct precipitation and run-off at the coring location, changes in the IWM could
517 also influence Indus River discharge, ~~because snowmelt is a significant contributor in the~~
518 ~~upper Indus catchment (Karim et al., 2002) and peaks during the summer months (Yu et al.,~~
519 ~~2013).~~

520

521 The thermocline-dwelling foraminifera *N. dutertrei* shows maximum abundances during
522 winter, and are interpreted to reflect winter mixing. ~~Weaker IWM winds are expected to~~
523 ~~result in a shorter duration and/or less intense upper ocean mixing, although how this signal~~
524 ~~is ultimately related to the amount or distribution of winter rainfall in the Indus River~~
525 ~~catchment has not been demonstrated conclusively. Dimri (2006) studied Western~~
526 ~~Disturbances for the time period 1958-1997, and noted that surplus years of winter~~
527 ~~precipitation are linked to significant heat loss over the northern Arabian Sea, which is mainly~~
528 ~~attributed to intensified westerly moisture flow and enhanced evaporation. Such conditions~~
529 ~~would promote deeper winter mixing, and provide a basis for relating thermocline depth with~~
530 ~~IWM intensity.~~ During weak IWM conditions, colder unmixed water would result in higher
531 $\delta^{18}\text{O}$ values of *N. dutertrei*, whereas enhanced mixing and homogenization of the water
532 column under strong IWM conditions would decrease $\delta^{18}\text{O}$. The minimum of $\delta^{18}\text{O}$ in *N.*
533 *dutertrei* occurs between 4.5 and 4.3 ka BP, pointing to a period of strengthened IWM. We
534 interpret the stepped increase in $\delta^{18}\text{O}$ of *N. dutertrei* at 4.1 ka BP to represent a decrease in
535 IWM wind-driven mixing. Similarly, $\delta^{13}\text{C}$ of *N. dutertrei* increases significantly after 4.1 ka BP

(Figure 37), which ~~would could also suggest~~ indicate reduced upwelling of low $\delta^{13}\text{C}$ intermediate water ~~under a weaker IWM~~ (Lynch-Stieglitz, 2006; Ravelo and Hillaire-Marcel, 2007; Sautter and Thunell, 1991); however, the interpretation of $\delta^{13}\text{C}$ remains uncertain because of a poor understanding of the controls on the $\delta^{13}\text{C}$ of planktonic foraminifera in this region. According to the $\delta^{18}\text{O}$ signal of *N. dutertrei*, the temperature pattern in the thermocline implies surface cooling between 4.5 and 4.3 ka BP and surface warming after 4.1 ka BP interrupted only by a period of cooling between 3.7 and 3.3 ka BP, which is in broad agreement with records of alkenone sea-surface temperature estimates from cores in the northeastern Arabian Sea ("E" in Figure 1) (Dooze-Rolinski et al., 2001; Staubwasser, 2012).

5.2 Interpretation of foraminifer $\Delta\delta^{18}\text{O}$

By using $\Delta\delta^{18}\text{O}$ between foraminifer species, we can distinguish additional processes affecting the surface waters and thermocline (Ravelo and Shackleton, 1995). This technique has been used previously to infer changes in the strength of the East Asian Winter Monsoon (EAWM) in the South China Sea (Tian et al., 2005), as well as mixed layer and thermocline depth in other studies (Billups et al., 1999; Cannariato and Ravelo, 1997; Norris, 1998). Here we use the difference in the $\delta^{18}\text{O}$ of *G. ruber* and *N. dutertrei* ($\Delta\delta^{18}\text{O}_{d-r}$) to track changes in the surface-to-deep gradient. This gradient can be driven by either $\delta^{18}\text{O}$ changes in the surface-dwelling (*G. ruber*) and/or the thermocline-dwelling species (*N. dutertrei*). During times of a strengthened winter monsoon, $\Delta\delta^{18}\text{O}_{d-r}$ will decrease as surface waters are homogenized and the thermocline deepens. Similarly, $\Delta\delta^{18}\text{O}_{d-r}$ will also decrease during times of a weakened summer monsoon, as decreased Indus River discharge will increase surface water salinity and $\delta^{18}\text{O}$ of *G. ruber* will become more similar to *N. dutertrei*.

G. sacculifer is also a surface dweller, but has a slightly deeper depth habitat than *G. ruber*. We thus expect *G. ruber* to be more influenced by surface salinity variations than *G. sacculifer*, and suggest the $\delta^{18}\text{O}$ difference between the two species ($\Delta\delta^{18}\text{O}_{s-r}$) reflects the influence of Indus River discharge on near surface salinity. The ~~greatest-smallest~~ difference in $\Delta\delta^{18}\text{O}_{s-r}$ occurs at 4.1 ka BP, which is interpreted as an increase in surface water salinity (Figure 68).

The difference in $\delta^{18}\text{O}$ between *G. sacculifer* and *N. dutertrei* ($\Delta\delta^{18}\text{O}_{d-s}$) also reflects surface mixing and thermocline depth, but *G. sacculifer* is less affected by surface salinity changes than *G. ruber*. Thus, the responses of $\Delta\delta^{18}\text{O}_{s-d-rs}$ and $\Delta\delta^{18}\text{O}_{d-sr}$ can be used to differentiate between surface water salinity changes and wind-driven mixing. Accordingly, simultaneously low $\Delta\delta^{18}\text{O}_{d-s}$ and $\Delta\delta^{18}\text{O}_{d-r}$ indicate a period of increased surface water mixing and increased IWM (such as the period between 4.5 and 4.3 ka BP), but times of relatively low $\Delta\delta^{18}\text{O}_{d-s}$ but high $\Delta\delta^{18}\text{O}_{d-r}$ and $\Delta\delta^{18}\text{O}_{s-r}$ (around 5.0 ka BP) indicate periods of increased Indus discharge and strength of the ISM and IWM.

~~However, t~~The following period of low $\Delta\delta^{18}\text{O}_{d-r}$ but high $\Delta\delta^{18}\text{O}_{d-s}$ from 4.1-3.9 ka BP is likely driven by increased salinity of surface water. This distinction becomes clearer when examining the $\Delta\delta^{18}\text{O}_{s-r}$, where increased similarity from 4.8-3.9 ka BP (with a sharp increase at 4.1 ka BP) reflects the effect of increased sea surface salinity that reduces the $\delta^{18}\text{O}$ difference between *G. ruber* and *G. sacculifer*. At the same time, weakened winter mixing increases $\Delta\delta^{18}\text{O}_{d-s}$, which occurs from 4.2-3.9 ka BP. Importantly, the proxies also indicate that increased IWM mixing is generally positively correlated with increased Indus discharge, and

583 vice versa. The single time period when this does not hold true is 4.5-4.25 ka BP, when
584 increased IWM mixing is coupled with decreased Indus discharge.

585
586 In summary, our multi-species approach using $\delta^{18}\text{O}$ of *G. ruber*, *G. sacculifer*, and *N. dutertrei*
587 allows us to differentiate between strength of the IWM and freshwater discharge of the Indus
588 River. We suggest that ISM strength decreased gradually from at least 4.8 ka BP, while the
589 IWM strength peaked around 4.5-4.3 ka BP and then weakened afterwards. It is unlikely that
590 the abrupt increase in *G. ruber* $\delta^{18}\text{O}$ at 4.1 ka BP and low $\Delta\delta^{18}\text{O}_{s-r}$ could be caused solely by
591 the decrease in IWM strength, even though IWM contributes to Indus River discharge.
592 Weakening of the ISM must have played a substantial role in the 4.1 ka BP shift as well,
593 indicated by the period 4.5-4.25 ka BP, when Indus discharge reflected a weak ISM ($\Delta\delta^{18}\text{O}_{s-r}$)
594 despite a phase of strengthened IWM.

595

596 5.3 Comparison to marine records

597

598 ~~The interpretation of core 63KA relies on proxies that directly link surface water salinity to~~
599 ~~ISM precipitation and Indus River discharge, and thermocline shifts to related IWM driven~~
600 ~~mixing. Additionally, there is an established mechanism relating mixing with IWM strength,~~
601 ~~as anomalously cool and evaporative conditions over the northern Arabian Sea (promoting~~
602 ~~deeper winter mixing) correlates with increased winter precipitation in the western~~
603 ~~Himalayas (Dimri, 2006). The strength of the 63KA core lies in its highly resolved age model,~~
604 ~~high sedimentation rates and its position in particularly saline surface waters (ASHSW) close~~
605 ~~to highly contrasting freshwater sources. Additionally, both the ISM and IWM are co-~~
606 ~~registered in proxies in the same laminated core with no bioturbation, thereby permitting an~~
607 ~~explicit evaluation of the relative timing of the two monsoons.~~

608

609 Other marine records from the Arabian Sea also suggest a gradual decrease in ISM strength
610 since from ~5 ka BP (Gupta et al., 2003; Overpeck et al., 1996). Cullen et al. (2000) observed
611 an abrupt peak in aeolian dolomite and calcite in marine sediments in the Gulf of Oman from
612 4.0-3.6 ka BP, and Ponton et al. (2012) also showed a shift to weaker ISM after 4.0 ka BP in
613 the Bay of Bengal, based on $\delta^{13}\text{C}$ of leaf waxes. Marine IWM reconstructions are not
614 particularly coherent: although Dose-Rolinski et al. (2001) find a decrease in evaporation
615 and weakening of the ISM between 4.6 and 3.7 ka BP, they argue this was accompanied by a
616 relative increase in IWM strength. Giosan et al. (2018, in review) inferred enhanced winter
617 monsoon conditions from 4.5-3.0 ka BP based on a planktic paleo-DNA and % *Globigerina*
618 *falconensis* record close to our coring site ("C" in Figure 1), which contradicts-disagrees with
619 our finding of decreased upper ocean mixing after 4.3 ka BP. We suggest the-that the high
620 stratigraphic (i.e., laminated) and chronological (i.e., 15 radiocarbon dates between 5.4-3.0
621 ka BP) resolution of core 63KA paired with a multi-species foraminifer $\delta^{18}\text{O}$ record can
622 provides a more detail about robust history of the timing of changes in IWM and ISM strength,
623 but additional studies are needed to resolve some of the discrepancies among the records.

624

625 5.4 Comparison to regional terrestrial records

626

627 The 63KA $\delta^{18}\text{O}$ record obtained from three foraminifer species highlights several important
628 ocean-atmosphere changes over the 5.4-3.0 ka BP time period. First, a sharp decrease
629 occurred in both summer and winter precipitation at 4.1 ka BP, which is within a broader 300-

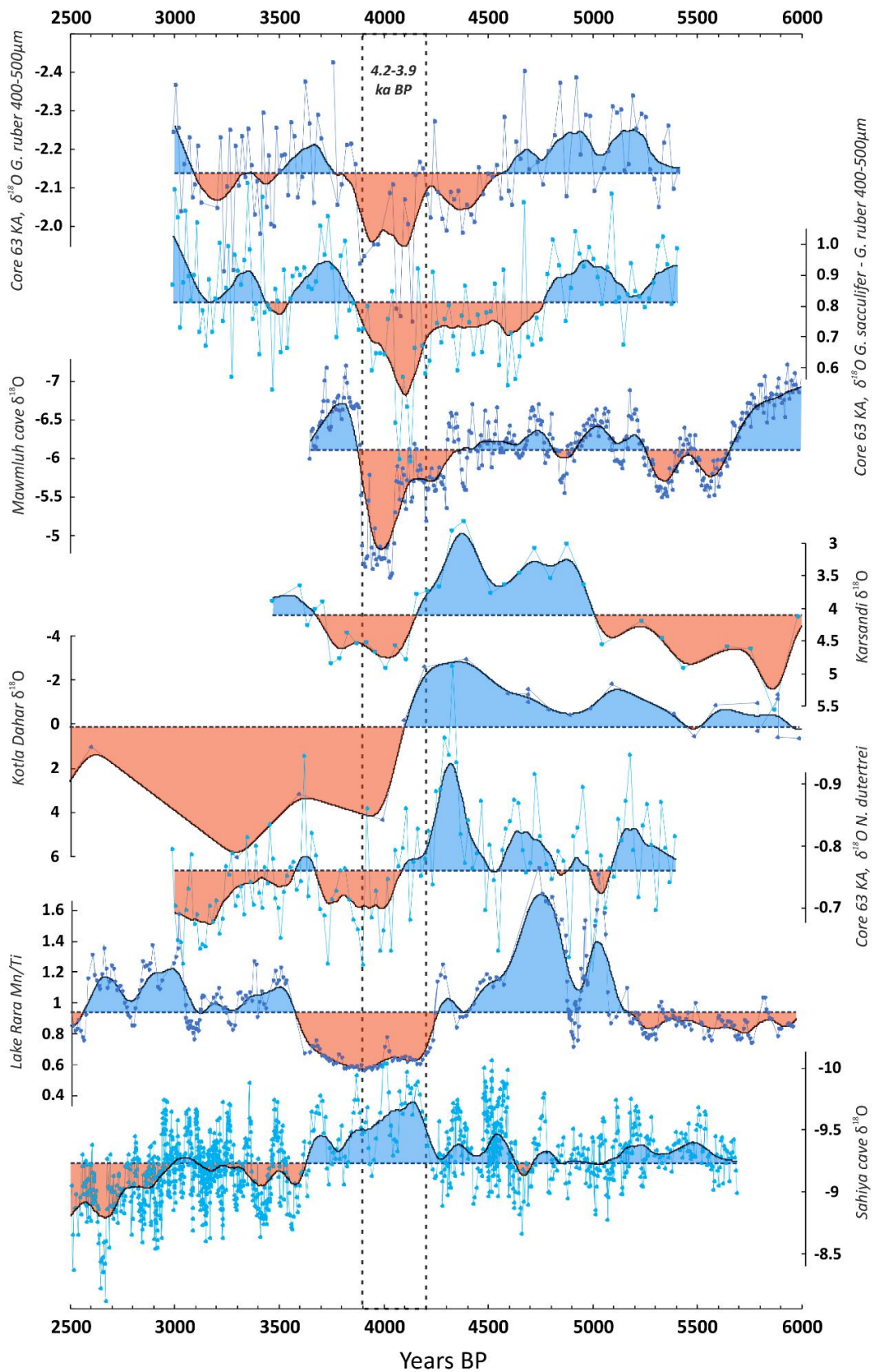
630 year period of increased aridity spanning both rainfall seasons between 4.2 and 3.9 ka BP. In
631 detail, we infer a relative decrease in Indus River discharge and weakened ISM between 4.8
632 and 3.9 ka BP, peaking at 4.1 ka BP, while a 200-year-long ~~phase interval~~ of strong IWM
633 interrupted this period from 4.5-4.3 ka BP. Furthermore, the stepped change in $\delta^{18}\text{O}$ of *N.*
634 *dutertrei* suggests an enduring change in ocean-atmosphere conditions after 4.1 ka BP.

635
636 A relatively abrupt ~ 4.2 ka BP climate event has been observed in several terrestrial records
637 on the Indian subcontinent, most notably Mawmluh Cave (~ 4.1 -3.9 ka BP) in northeastern
638 India (Berkelhammer et al., 2012) and Kotla Dahar (~ 4.1 ka BP) in northwestern India (Dixit et
639 al., 2014) (Figure 79). A less abrupt yet still arid period is documented in a peat profile (~ 4.0 -
640 3.5 ka BP) from northcentral India (Phadtare, 2000), at Lonar Lake (~ 4.6 -3.9 ka BP) in central
641 India (Menzel et al., 2014), and at Rara Lake (~ 4.2 -3.7 ka BP) in western Nepal (Nakamura et
642 al., 2016). Finally, a recent study of oxygen and hydrogen isotopes in gypsum hydration water
643 from Karsandi on the northern margin of the Thar Desert showed wet conditions between 5.1
644 and 4.4 ka BP, after which the playa lake dried out sometime between 4.4 and 3.2 ka BP (Dixit
645 et al., 2018). Considering terrestrial records can record more local climatic conditions than
646 marine records, it is remarkable that the records collectively agree on a ~~regional phase period~~
647 of ~~regional~~ aridity between 4.2 and 3.9 ka BP within the uncertainties of the age models that
648 vary considerably among records.

649
650 However, not all records support this finding, ~~such as~~ for example, a reconstruction from
651 Sahiya Cave in northwestern India ~~that~~ shows an abrupt decrease in $\delta^{18}\text{O}$ interpreted to
652 reflect an increase in monsoon strength from ~ 4.3 -4.15 ka BP, followed by an arid trend after
653 4.15 ka BP (Kathayat et al., 2017). In addition, several other Thar Desert records do not
654 identify a “4.2 ka BP event” *sensu stricto*, but instead suggest that lakes dried out several
655 centuries earlier (Deotare et al., 2004; Enzel et al., 1999; Singh et al., 1990) or later (Sinha et
656 al., 2006) than 4.2 ka BP. This discrepancy may relate to non-linear climate responses of lakes,
657 which would not record a drought at 4.2 ka BP if they had already dried out earlier from the
658 ongoing decrease in summer rainfall. In addition, there are also significant concerns about
659 chronological uncertainties ~~when using~~ from the use of radiocarbon of bulk sediment for
660 dating in some of these records. It is also possible that variations in the timing of climate
661 change inferred from the terrestrial records may be real, reflecting different sensitivity to ISM
662 and IWM rain. As a marine record, core 63KA integrates large-scale ocean-atmosphere
663 changes, and therefore can help inform the interpretation of the more locally sensitive
664 terrestrial records.

665
666 More distantly, several terrestrial records in the Middle East also show a decrease in winter
667 precipitation proxies around 4.2 ka BP: Jeita Cave in Lebanon records a relatively dry period
668 between 4.4 and 3.9 ka BP (Cheng et al., 2015) and Soreq Cave in Israel shows a period of
669 increased aridity starting at ~ 4.3 ka BP (Bar-Matthews et al., 2003; Bar-Matthews and Ayalon,
670 2011) (Figure 84). Lake Van in eastern Turkey also records reduced spring rainfall and
671 enhanced aridity after ~ 4.0 ka BP (Wick et al., 2003; Lemcke and Sturm, 1997). All of these
672 records suggest a relatively arid ~~phase period in with reduced~~ winter precipitation after ~ 4.3
673 ka BP, as inferred from core 63-KA. Qunf Cave in Oman (Fleitmann et al., 2003), which is
674 outside the range of IWM influence, instead shows a steady mid-Holocene weakening of the
675 ISM that closely follows trends in summer solar insolation. ~~Core 63 KA also infers a protracted~~
676 ~~decrease in ISM since ~ 4.8 ka BP.~~

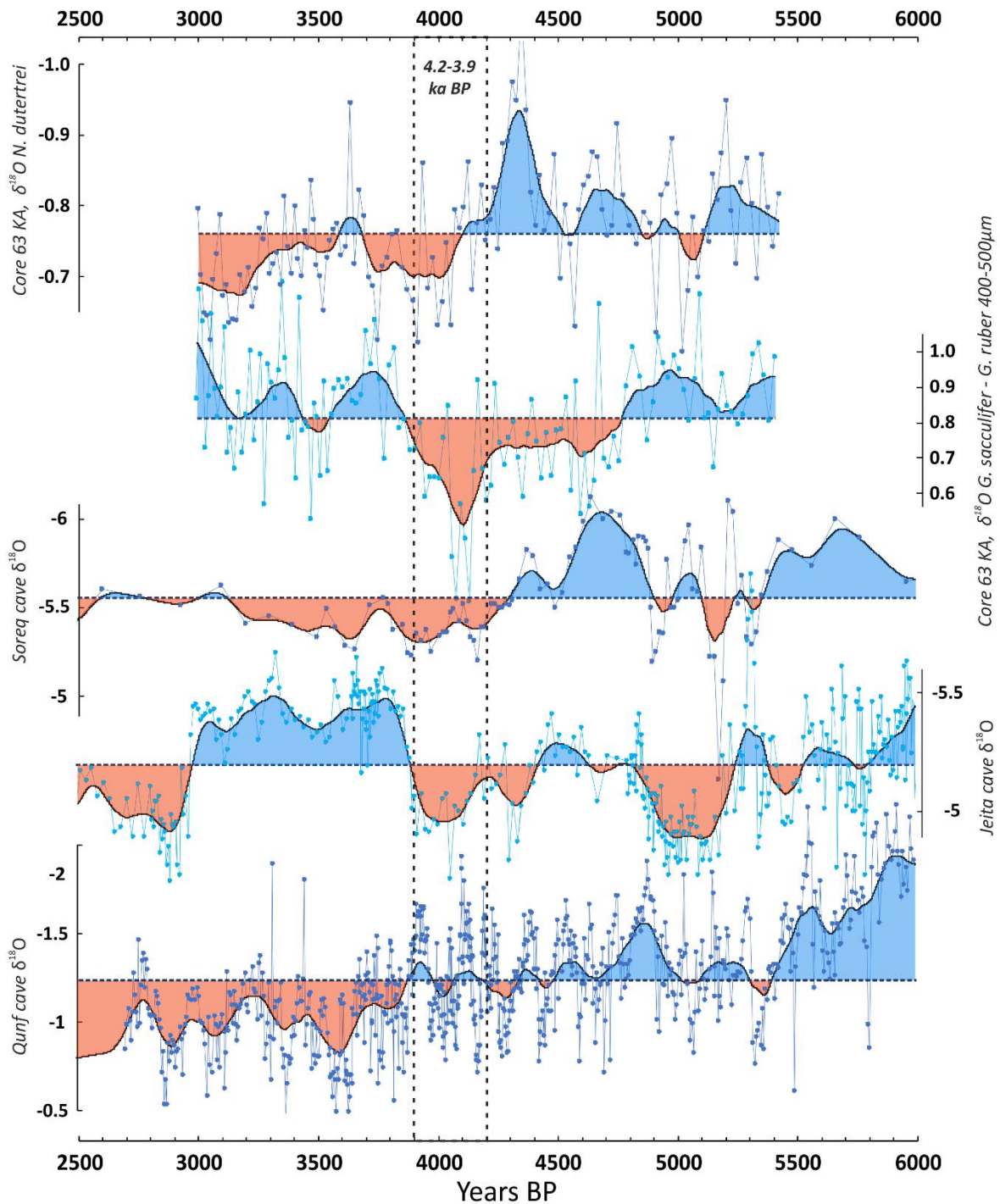
677
678



679
680
681

Figure 79. Comparison of the $\delta^{18}\text{O}$ record of core 63KA with terrestrial records from the Indian Subcontinent, from top to bottom: this study (first two), Berkelhammer et al., 2012; Dixit et al., 2018;

682 Dixit et al., 2014; this study; Nakamura et al., 2016; Kathayat et al., 2017. The mean value for each
 683 record indicated by the horizontal dashed lines is taken for all available data between 6.0-2.5 ka BP.
 684



685
 686 **Figure 810.** Comparison of the $\delta^{18}\text{O}$ record of core 63KA (topmost records),
 687 from top to bottom: Bar-Matthews et al., 2003; Cheng et al., 2015; and Fleitmann et al., 2003. Mean
 688 The mean value for each record indicated by the horizontal dashed lines is taken for all available data
 689 between 6.0-2.5 ka BP.

690
 691 5.5 Cultural impacts

692

693 ~~Based on~~ On the basis of our reconstruction of reduced IWM mixing after 4.3 ka BP,
694 accompanied by decreased freshwater discharge of the Indus River, it is worth considering
695 what impacts could be expected from a reduction in IWM and ISM precipitation. A weakened
696 IWM overlying a reduced or more variable ISM would likely result in a distinct climate signal
697 over the Indus River catchment, with broad implications for seasonal river flow and water
698 availability throughout the year. The presence of the two rainfall systems creates a complex
699 and diverse range of environments and ecologies across northwest South Asia (Petrie et al.,
700 2017). In a situation when rainfall in both seasons is reduced over extended periods, step-
701 shifts in the natural environment may occur that are difficult to reverse (e.g., desertification,
702 lake desiccation, regional vegetation changes, decline in overbank flooding and shift in river
703 avulsion patterns).

704
705 Societies reliant on IWM, ISM, or a combination of the two would have been vulnerable to
706 years with monsoon failure, and a shift affecting both seasons will have challenged resilience
707 and tested sustainability (Green and Bates et al. in ~~prepress~~; Petrie et al., 2017).
708 Archaeological research into the transition from the urban Mature Harappan phase (~4.6-3.9
709 ka BP) to the post-urban Late Harappan phase (~3.9-3.6 ka BP) notes progressive
710 deurbanization through the abandonment of large Indus cities and a depopulation of the
711 most western Indus regions, concurrent with a general trend towards an increase of
712 concentrations of rural settlements in some areas of the eastern Indus extent (Green and
713 Petrie, 2018; Petrie et al., 2017; Possehl, 1997) (Figure S6). The relatively limited range of
714 well-resolved available archaeobotanical data suggests that there was a degree of diversity in
715 crop choice and farming strategies in different parts of the Indus Civilization across this time
716 span (Petrie et al., 2016; Petrie and Bates, 2017; Weber, 1999; Weber et al., 2010). Farmers
717 in southerly regions appear to have focused on summer or winter crops, while the more
718 northern regions of Pakistan Punjab and Indian Punjab and Haryana were capable of
719 supporting combinations of winter and summer crops (Petrie and Bates, 2017). Although
720 there is evidence for diverse cropping practices involving both summer and winter crops in
721 the northern areas during the urban period, agricultural strategies appeared to favor more
722 intensive use of drought-resistant summer crops in the Late Harappan period (Madella and
723 Fuller, 2006; Petrie and Bates, 2017; Pokharia et al., 2017; Weber, 2003; Wright, 2010). It has
724 previously been suggested that weakened ISM was a major factor in these shifts (e.g. Giosan
725 et al., 2012; Madella and Fuller, 2006). ~~On the basis of~~ Based on our reconstruction of
726 decreased IWM in northwest South Asia after 4.3 ka BP with a step-shift at 4.1 ka BP, we
727 suggest that both IWM and ISM climatic factors played a role in shaping the human landscape.
728 This includes the redistribution of population to smaller settlements in eastern regions with
729 more direct summer rain, as well as the ~~observed~~ shift to more-increased summer crop
730 dominated cropping strategies.

731 732 **6. Conclusion**

733
734 This study expanded on the $\delta^{18}\text{O}$ record of planktonic foraminifer in core 63KA of the
735 northeastern Arabian Sea, originally published by Staubwasser et al. (2003). Using $\delta^{18}\text{O}$ of the
736 surface-dwelling foraminifera *G. ruber*, the original study inferred an abrupt reduction in
737 Indus River discharge at ~4.2 ka BP. Our further $\delta^{18}\text{O}$ analysis of a larger size fraction of this
738 species confirmed-corroborates maximum salinity at 4.1 and 3.95 ka BP. In addition, the $\delta^{18}\text{O}$
739 difference between the surface-dwelling *G. ruber* and slightly deeper-dwelling *G. sacculifer*

740 ($\Delta\delta^{18}\text{O}_{\text{s-r}}$) reveals that surface waters were more saline than average for the period from 4.8-
741 3.9 ka BP. By also measuring a thermocline-dwelling planktonic foraminiferal species, *N.*
742 *dutertrei*, we infer an increase in the strength of the IWM between 4.5 and 4.3 ka BP, followed
743 by reduction in IWM-driven mixing that ~~peaks~~ reaches a minimum at 4.1 ka BP.

744

745 Assuming that weaker IWM mixing implies a reduction in IWM rainfall amount or duration
746 over northwest South Asia under past climatic conditions, the 63KA core is used to infer
747 important changes in seasonal hydrology of the Indus River catchment. We propose that a
748 combined weakening of the IWM and ISM at 4.1 ka BP led to what has been termed the “4.2
749 ka BP” drought over northwest South Asia. The intersection of both a gradually weakening
750 ISM since 4.8 ka BP and a maximum decrease in IWM strength at 4.1 ka BP resulted in a
751 spatially layered and heterogeneous drought over a seasonal to annual timescale. Regions in
752 the western part of the Indus River basin accustomed to relying mainly on winter rainfall (also
753 via river run-off) would have been most severely affected by such changes. Regions in the
754 northeastern and eastern extents benefitted more from summer rainfall, and would have
755 been less severely affected, particularly as the ISM appears to recover strength by 3.9 ka BP.

756

757 Relatively strengthened IWM surface water mixing between 4.5 and 4.3 ka BP correlates with
758 a period of higher precipitation recorded at Karsandi on the northern margin of the Thar
759 Desert (Dixit et al., 2018), an area within the summer rainfall zone that is also sensitive to
760 small changes in winter precipitation. This time span also represents the beginnings of the
761 Mature Harappan phase (Possehl, 2002; Wright, 2010), which implies that increasingly
762 urbanized settlements may have flourished under a strengthened IWM. With a weakening of
763 the IWM at ~4.1 ka, eastern regions with more access to ISM rainfall may have been more
764 favorable locations for agriculture. This may also help explain the broad shift in population
765 towards more rural settlements in the northeastern extent of the Indus Civilization that
766 occurred by ~3.9 ka BP (Possehl, 1997; Petrie et al., 2017), and a shift to more drought-
767 tolerant kharif (summer) season crops in Gujarat (Pokharia et al., 2017) and at Harappa
768 (Madella and Fuller, 2006; Weber, 2003).

769

770 Given the importance of the relationships between humans and the environment during the
771 time of the Indus Civilization, understanding the impact of the IWM on precipitation
772 variability in northwest South Asia remains a critical area of research. We especially need a
773 better understanding of the wind patterns and moisture pathways that controlled the IWM
774 in the past. Disentangling both the length and intensity of seasonal precipitation is a crucial
775 aspect of understanding the impact of climate change on past societies, particularly in a
776 diverse region relying on mixed water sources (e.g., fluvial, ground aquifer, direct rainfall).

777

778 **Data availability**

779

780 Data presented in the paper can be accessed by contacting the corresponding author at
781 ag927@cam.ac.uk. After final acceptance of the manuscript, the data will also be uploaded
782 to an online database.

783

784 **Author contributions**

785

786 M.S. supplied core 63KA material, A.G. prepared the material for isotopic measurements, and
787 A.G. and D.A.H. interpreted the results. A.G., D.A.H., and C.A.P. wrote the manuscript.

788

789 **Competing interests**

790

791 The authors declare that they have no conflict of interest.

792

793 **Acknowledgements**

794

795 This ~~work~~ research was carried out as part of the *TwoRains* project, which is supported by the
796 ERC-funded *TwoRains* project funding from the European Research Council (ERC) under the
797 European Union's Horizon 2020 research and innovation programme (grant agreement no
798 648609). The authors thank the following persons at the University of Cambridge: Maryline
799 Vautravers for foraminifera identification, James Rolfe and John Nicolson for $\delta^{18}\text{O}$
800 measurements. We also thank our editor and reviewers for comments that improved the
801 manuscript.

802

803 **References**

804

- 805 Agrawal, D. P.: The Indus Civilization: an interdisciplinary perspective, Aryan Books
806 International, New Delhi, India, 2007.
- 807 Ahmad, N., Mohammad, A., and Khan, S. T.: Country Report on Water resources of Pakistan,
808 in South Asia Water Balance Workshop. Hansen Institute for World Peace, San Diego,
809 California, USA, 30 April – 2 May 2001, 2001.
- 810 Banse, K.: Overview of the hydrography and associated biological phenomena in the Arabian
811 Sea off Pakistan, in Marine Geology and Oceanography of the Arabian Sea and Coastal
812 Pakistan, Ed. Haq, B. U., and Milliman, J. D., pp. 273-301, Van Nostrand Reinhold, New
813 York, 1984.
- 814 Bar-Matthews, M., and Ayalon, A.: Mid-Holocene climate variations revealed by high-
815 resolution speleothem records from Soreq Cave, Israel and their correlation with cultural
816 changes, *The Holocene*, 21, 163-171, 2011.
- 817 Bar-Matthews, M., Ayalon, A., Gilmour, M., Matthews, A., and Hawkesworth, C. J.: Sea-land
818 oxygen isotopic relationships from planktonic foraminifera and speleothems in the
819 Eastern Mediterranean region and their implication for paleorainfall during interglacial
820 intervals, *Geochimica et Cosmochimica Acta*, 67, 3181-3199, 2003.
- 821 Bé, A. W., and Hutson, W. H.: Ecology of planktonic foraminifera and biogeographic patterns
822 of life and fossil assemblages in the Indian Ocean, *Micropaleontology*, 369-414, 1977.
- 823 Bemis, B. E., Spero, H. J., Bijma, J., and Lea, D. W.: Reevaluation of the oxygen isotopic
824 composition of planktonic foraminifera: Experimental results and revised
825 paleotemperature equations. *Paleoceanography*, 13, 150-160, 1998.
- 826 Berkelhammer, M., Sinha, A., Stott, L., Cheng, H., Pausata, F. S., and Yoshimura, K.: An
827 abrupt shift in the Indian monsoon 4000 years ago, *Geophys. Monogr. Ser.*, 198, 2012.
- 828 Billups, K., Ravelo, A. C., Zachos, J. C., and Norris, R. D.: Link between oceanic heat transport,
829 thermohaline circulation, and the Intertropical Convergence Zone in the early Pliocene
830 Atlantic, *Geology*, 27, 319-322, 1999.
- 831 Blaauw, M., and Christen, J. A.: Flexible paleoclimate age-depth models using an
832 autoregressive gamma process, *Bayesian analysis*, 6, 457-474, 2011.

833 [Chaudhuri, P., and Marron, J. S.: SiZer for exploration of structures in curves, *Journal of the*](#)
834 [American Statistical Association, 94, 807-823, 1999.](#)

835 Cheng, H., Sinha, A., Verheyden, S., Nader, F. H., Li, X. L., Zhang, P. Z., Yin, J. J., Yi, L., Peng., Y.
836 B., Rao, Z. G., Ning, Y. F., and Edwards, R. L.: The climate variability in northern Levant
837 over the past 20,000 years, *Geophysical Research Letters*, 42, 8641-8650, 2015.

838 Cannariato, K.G., and Ravelo, A.C.: Pliocene-Pleistocene evolution of eastern tropical Pacific
839 surface water circulation and thermocline depth. *Paleoceanography*, 12, 805-820, doi:
840 10.1029/97PA02514, 1997.

841 Cayre, O., and Bassinot, F.: Oxygen isotope composition of planktonic foraminiferal shells
842 over the Indian Ocean: calibration to modern oceanographic data. *Mineral Mag*, 62, 288-
843 289, 1998.

844 Curry, W. B., Ostermann, D. R., Guptha, M. V. S., and Ittekkot, V.: Foraminiferal production
845 and monsoonal upwelling in the Arabian Sea: evidence from sediment traps, *Geological*
846 *Society, London, Special Publications*, 64, 93-106, 1992.

847 Cullen, H. M., deMenocal, P. B., Hemming, S., Hemming, G., Brown, F. H., Guilderson, T., and
848 Sirocko, F.: Climate change and the collapse of the Akkadian empire: Evidence from the
849 deep sea, *Geology*, 28, 379-382, 2000.

850 Dahl, K. A., and Oppo, D. W.: Sea surface temperature pattern reconstructions in the
851 Arabian Sea, *Paleoceanography*, 21, 2006.

852 Deotare, B. C., Kajale, M. D., Rajaguru, S. N., Kusumgar, S., Jull, A. J. T., and Donahue, J. D.:
853 Palaeoenvironmental history of Bap-Malar and Kanod playas of western Rajasthan, Thar
854 desert, *Journal of Earth System Science*, 113, 403-425, 2004.

855 Dimri, A. P.: Surface and upper air fields during extreme winter precipitation over the
856 western Himalayas, *Pure and Applied Geophysics*, 163, 1679-1698, 2006.

857 Dimri, A. P., and Dash, S. K.: Wintertime climatic trends in the western Himalayas. *Climatic*
858 *Change*, 111, 775-800, 2012.

859 Dixit, Y., Hodell, D. A., and Petrie, C. A.: Abrupt weakening of the summer monsoon in
860 northwest India ~4100 yr ago, *Geology*, 42, 339-342, 2014.

861 Dixit, Y., Hodell, D. A., Giesche, A., Tandon, S. K., Gázquez, F., Saini, H. S., Skinner, L. C.,
862 Mujtaba, S. A. I., Pawar, V., Singh, R.N., and Petrie, C. A.: Intensified summer monsoon
863 and the urbanization of Indus Civilization in northwest India, *Scientific reports*, 8, 4225,
864 2018.

865 Dooze-Rolinski, H., Rogalla, U., Scheeder, G., Lückge, A., and Rad, U.: High-resolution
866 temperature and evaporation changes during the late Holocene in the northeastern
867 Arabian Sea, *Paleoceanography and Paleoclimatology*, 16, 358-367, 2001.

868 Duplessy, J. C., Labeyrie, L., Arnold, M., Paterne, M., Duprat, J., and van Weering, T. C.:
869 Changes in surface salinity of the North Atlantic Ocean during the last deglaciation.
870 *Nature*, 358, 485, 1992.

871 Enzel, Y., Ely, L. L., Mishra, S., Ramesh, R., Amit, R., Lazar, B., Rajaguru, S.N., Baker, V. R., and
872 Sandler, A.: High-resolution Holocene environmental changes in the Thar Desert,
873 northwestern India, *Science*, 284, 125-128, 1999.

874 Farmer, E. C., Kaplan, A., de Menocal, P. B., and Lynch-Stieglitz, J.: Corroborating ecological
875 depth preferences of planktonic foraminifera in the tropical Atlantic with the stable
876 oxygen isotope ratios of core top specimens, *Paleoceanography*, 22, 2007.

877 Finné, M., Holmgren, K., Sundqvist, H. S., Weiberg, E., and Lindblom, M.: Climate in the
878 eastern Mediterranean, and adjacent regions, during the past 6000 years—A review,
879 *Journal of Archaeological Science*, 38, 3153-3173, 2011.

880 Fleitmann, D., Burns, S. J., Mudelsee, M., Neff, U., Kramers, J., Mangini, A., and Matter, A.:
881 Holocene forcing of the Indian monsoon recorded in a stalagmite from southern Oman,
882 Science, 300, 1737-1739, 2003.

~~883 Fleitmann, D., Burns, S. J., Mangini, A., Mudelsee, M., Kramers, J., Villa, I., Neff, U., Al-~~
884 ~~Subbary, A. A., Buettner, A., Hippler, D., and Matter, A.: Holocene ITCZ and Indian~~
885 ~~monsoon dynamics recorded in stalagmites from Oman and Yemen (Socotra), Quaternary~~
886 ~~Science Reviews, 26, 170-188, 2007.~~

887 Gadgil, S.: The Indian monsoon and its variability, Annual Review of Earth and Planetary
888 Sciences, 31, 429-467, 2003.

889 Giosan, L., Clift, P. D., Macklin, M. G., Fuller, D. Q., Constantinescu, S., Durcan, J. A., Stevens,
890 T., Duller, G. A. T., Tabrez, A. R., Gangal, K., Adhikari, R., Alizai, A., Filip, F., VanLaningham,
891 S., and Syvitski, J. P. M.: Fluvial landscapes of the Harappan civilization, Proceedings of
892 the National Academy of Sciences, 109, E1688-E1694, 2012.

893 Giosan, L., Orsi, W. D., Coolen, M., Wuchter, C., Dunlea, A. G., Thirumalai, K., Munoz, S. E.,
894 Clift, P. D., Donnelly, J. P., Galy, V., and Fuller, D. Q.: Neoglacial Climate Anomalies and
895 the Harappan Metamorphosis, *Climate of the Past*, 14, 1669-1686, ~~-Past Discuss.,~~
896 ~~doi:10.5194/cp-2018-37, in review,~~ 2018.

897 Green, A. S., Bates, J., Acabado, S., Coutros, P., Glover, J., Miller, N., Sharratt, N., and Petrie,
898 C.A.: How to Last a Millennium; Or a Global Perspective on the Long-Term Dynamics of
899 Human Sustainability, in ~~preparation press (under review)~~ for Nature Sustainability.

900 Green, A. S., and Petrie, C. A.: Landscapes of Urbanization and De-Urbanization: A Large-
901 Scale Approach to Investigating the Indus Civilization's Settlement Distributions in
902 Northwest India, *Journal of Field Archaeology*, 1-16, 2018.

903 Gupta, A. K., Anderson, D. M., and Overpeck, J. T.: Abrupt changes in the Asian southwest
904 monsoon during the Holocene and their links to the North Atlantic Ocean. *Nature*, 421,
905 354, 2003.

906 Hastenrath, S., and Lamb, P. J.: Climatic atlas of the Indian Ocean. Part II: The oceanic heat
907 budget, Wisconsin University Press, Madison, Wisconsin, USA, 93, 17, 1979.

908 Hatwar, H. R., Yadav, B. P., and Rao, Y. R.: Prediction of western disturbances and associated
909 weather over Western Himalayas, *Current science*, 913-920, 2005.

910 Hemleben, C., Spindler, M., and Anderson, O. R.: Modern planktonic foraminifera. Springer
911 Science and Business Media, 2012.

912 Joseph, S., and Freeland, H. J.: Salinity variability in the Arabian Sea. *Geophysical research*
913 *letters*, 32, 2005.

914 Karim, A., and Veizer, J.: Water balance of the Indus River Basin and moisture source in the
915 Karakoram and western Himalayas: Implications from hydrogen and oxygen isotopes in
916 river water, *Journal of Geophysical Research: Atmospheres*, 107, ACH-9, 2002.

917 Kathayat, G., Cheng, H., Sinha, A., Yi, L., Li, X., Zhang, H., Li, H., Ning, Y., and Edwards, R. L.:
918 The Indian monsoon variability and civilization changes in the Indian subcontinent,
919 *Science advances*, 3, e1701296, 2017.

920 Kim, S. T., and O'Neil, J. R.: Equilibrium and nonequilibrium oxygen isotope effects in
921 synthetic carbonates, *Geochimica et Cosmochimica Acta*, 61, 3461-3475, 1997.

922 Kumar, S. P., and Prasad, T. G.: Formation and spreading of Arabian Sea high-salinity water
923 mass, *Journal of Geophysical Research: Oceans*, 104, 1455-1464, 1999.

924 Lemcke, G., and Sturm, M.: $\delta^{18}\text{O}$ and trace element measurements as proxy for the
925 reconstruction of climate changes at Lake Van (Turkey): Preliminary results, in Third

926 millennium BC climate change and Old World collapse, Springer, Berlin, Heidelberg,
927 Germany, 653-678, 1997.

928 [Locarnini, R. A., Mishonov, A. V., Antonov, J. I., Boyer, T. P., Garcia, H. E., Baranova, O. K.,](#)
929 [Zweng, M. M., Paver, C. R., Reagan, J. R., Johnson, D. R., Hamilton, M., and Seidov, D.:](#)
930 [World Ocean Atlas 2013, Volume 1: Temperature. S. Levitus, Ed., A. Mishonov Technical](#)
931 [Ed., NOAA Atlas NESDIS 73, 40 pp., 2013.](#)

932 Lynch-Stieglitz, J.: Tracers of past ocean circulation, in: Treatise on geochemistry, 6,
933 Elderfield, H., Holland, H. D., and Turekian, K. K. (Eds), Elsevier, 433-451, 2006.

934 Madella, M., and Fuller, D. Q.: Palaeoecology and the Harappan Civilisation of South Asia: a
935 reconsideration, Quaternary Science Reviews, 25, 1283-1301, 2006.

936 [Madhupratap, M., Kumar, S. P., Bhattathiri, P. M. A., Kumar, M. D., Raghukumar, S., Nair, K.](#)
937 [K. C., and Ramaiah, N.: Mechanism of the biological response to winter cooling in the](#)
938 [northeastern Arabian Sea, Nature, 384, 549-552, 1996.](#)

939 Maslin, M. A., Shackleton, N. J., and Pflaumann, U.: Surface water temperature, salinity, and
940 density changes in the northeast Atlantic during the last 45,000 years: Heinrich events,
941 deep water formation, and climatic rebounds, Paleoceanography, 10, 527-544, 1995.

942 Mayewski, P. A., Rohling, E. E., Stager, J. C., Karlén, W., Maasch, K. A., Meeker, L. D.,
943 Meyerson, E. A., Gasse, F., van Kreveld, S., Holmgren, K., Lee-Thorp, J., Rosqvist, G., Rack,
944 F., Staubwasser, M., Schneider, R.R., and Steig, E.J.: Holocene climate variability,
945 Quaternary research, 62, 243-255, 2004.

946 Menzel, P., Gaye, B., Mishra, P. K., Anoop, A., Basavaiah, N., Marwan, N., Plessen, B., Prasad,
947 S., Riedel, N., Stebich, M., and Wiesner, M. G.: Linking Holocene drying trends from Lonar
948 Lake in monsoonal central India to North Atlantic cooling events, Palaeogeography,
949 palaeoclimatology, palaeoecology, 410, 164-178, 2014.

950 Nakamura, A., Yokoyama, Y., Maemoku, H., Yagi, H., Okamura, M., Matsuoka, H., Miyake,
951 N., Osada, T., Adhikari, D. P., Dangol, V., Ikehara, M., Miyairi, Y., and Matsuzaki, H.: Weak
952 monsoon event at 4.2 ka recorded in sediment from Lake Rara, Himalayas, Quaternary
953 International, 397, 349-359, 2016.

954 Norris, R. D.: Planktonic foraminifer biostratigraphy: eastern equatorial Atlantic, in:
955 Proceedings of the Ocean Drilling Program: Scientific results, 159, 445-479, 1998.

956 Overpeck, J., Anderson, D., Trumbore, S., and Prell, W.: The southwest Indian Monsoon over
957 the last 18000 years. Climate Dynamics, 12, 213-225, 1996.

958 Petrie, C. A., and Bates, J.: 'Multi-cropping', Intercropping and Adaptation to Variable
959 Environments in Indus South Asia. Journal of World Prehistory, 30, 81-130, 2017.

960 Petrie, C. A., Bates, J., Higham, T., and Singh, R. N.: Feeding ancient cities in South Asia:
961 dating the adoption of rice, millet and tropical pulses in the Indus civilisation. Antiquity,
962 90, 1489-1504, 2016.

963 Petrie, C. A., Singh, R. N., Bates, J., Dixit, Y., French, C. A., Hodell, D. A., Pandey, A. K., Parikh,
964 D., Pawar, V., Redhouse, D. I., and Singh, D. P.: Adaptation to variable environments,
965 resilience to climate change: Investigating land, water and settlement in Indus Northwest
966 India, Current Anthropology, 58, 2017.

967 Phadtare, N. R.: Sharp decrease in summer monsoon strength 4000–3500 cal yr BP in the
968 Central Higher Himalaya of India based on pollen evidence from alpine peat, Quaternary
969 Research, 53, 122-129, 2000.

970 Pokharia, A. K., Agnihotri, R., Sharma, S., Bajpai, S., Nath, J., Kumaran, R. N., and Negi, B. C.:
971 Altered cropping pattern and cultural continuation with declined prosperity following

972 abrupt and extreme arid event at ~4,200 yrs BP: Evidence from an Indus archaeological
973 site Khirsara, Gujarat, western India, PloS one, 12, 2017.

974 Ponton, C., Giosan, L., Eglinton, T. I., Fuller, D. Q., Johnson, J. E., Kumar, P., and Collett, T. S.:
975 Holocene aridification of India, Geophysical Research Letters, 39, 2012.

976 Possehl, G. L.: The transformation of the Indus civilization, Journal of World Prehistory, 11,
977 425-472, 1997.

978 Possehl, G. L.: The Indus Civilization: a Contemporary Perspective. Rowman Altamira, 2002.

979 Possehl, G. L.: The Indus Civilization: an introduction to environment, subsistence, and
980 cultural history. Indus ethnobiology, 1-20, 2003.

981 Prasad, S., and Enzel, Y.: Holocene paleoclimates of India. Quaternary Research, 66, 442-
982 453, 2006.

983 Ramasastri, K.S.: Snow melt modeling studies in India, in: The Himalayan Environment, S.K.
984 Dash and J. Bahadur (Eds.), New Age International, 59–70, 1999.

985 Rangachary, N., and Bandyopadhyay, B. K.: An analysis of the synoptic weather pattern
986 associated with extensive avalanching in Western Himalaya, Int. Assoc. of Hydrol. Sci.
987 Publ, 162, 311-316, 1987.

988 ~~Rao, Y.P.: The Climate of the Indian Sub-Continent, in: World Survey of Climatology, 9,
989 Climates of Southern and Western Asia, Elsevier, Amsterdam, Netherlands, 67-182, 1981.~~

990 Ravelo, A. C., and Hillaire-Marcel, C.: Chapter Eighteen the use of oxygen and carbon
991 isotopes of foraminifera in Paleoceanography, Developments in Marine Geology, 1, 735-
992 764, 2007.

993 Ravelo, A.C., and Shackleton, N.J.: Evidence for surface-water circulation changes at Site 851
994 in the eastern Tropical Pacific Ocean, in: Proceedings of the Ocean Drilling Program,
995 Scientific Results, College Station, TX (Ocean Drilling Program), Pisias, N. G.; Mayer, L. A.;
996 Janecek, T. R.; Palmer-Julson, A.; van Andel, T. H. (Eds.), 138, 503-514, doi:
997 10.2973/odp.proc.sr.138.126, 1995.

998 Reimer, P. J., Bard, E., Bayliss, A., Beck, J. W., Blackwell, P. G., Ramsey, C. B., Buck, C. E.,
999 Cheng, H., Edwards, R. L., Friedrich, M., Grootes, P. M., Guilderson, T. P., Haflidason, H.,
1000 Hajdas, I., Hatté, C., Heaton, T. J., Hoffmann, D. L., Hogg, A. G., Hughen, K. A., Kaiser, K. F.,
1001 Kromer, B., Manning, St.W., Niu, M., Reimer, R. W., Richards, D. A., Scott, E. M., Southon,
1002 J. R., Staff, R. A., Turney, C. S. M., and van der Plicht, J.: IntCal13 and Marine13
1003 radiocarbon age calibration curves 0–50,000 years cal BP, Radiocarbon, 55, 1869-1887,
1004 2013.

1005 Rohling, E. J.: Paleosalinity: confidence limits and future applications, Marine Geology, 163,
1006 1-11, 2000.

1007 Sautter, L. R., and Thunell, R. C.: Seasonal variability in the $\delta^{18}\text{O}$ and $\delta^{13}\text{C}$ of planktonic
1008 foraminifera from an upwelling environment: sediment trap results from the San Pedro
1009 Basin, Southern California Bight. Paleoceanography, 6, 307-334, 1991.

1010 Schneider, U., Becker, A., Finger, P., Meyer-Christoffer, A., Bruno, R., and Ziese, M.: GPCP
1011 Full Data Reanalysis Version 7.0 at 0.5°: Monthly Land-Surface Precipitation from Rain-
1012 Gauges built on GTS-based and Historic Data, Deutscher Wetterdienst/Global
1013 Precipitation Climatology Centre, 2015.

1014 Schulz, H., von Rad, U., and Ittekkot, V.: Planktic foraminifera, particle flux and oceanic
1015 productivity off Pakistan, NE Arabian Sea: modern analogues and application to the
1016 palaeoclimatic record, Geological Society, London, Special Publications, 195, 499-516,
1017 2002.

- 1018 Shackleton, N. J.: Attainment of isotopic equilibrium between ocean water and the
1019 benthonic foraminifera genus *Uvigerina*: isotopic changes in the ocean during the last
1020 glacial, *Colloques Internationaux du C.N.R.S.*, 1974.
- 1021 Shenoj, S. S. C., Shankar, D., and Shetye, S. R.: Differences in heat budgets of the near-
1022 surface Arabian Sea and Bay of Bengal: Implications for the summer monsoon, *Journal of*
1023 *Geophysical Research: Oceans*, 107, 5-1, 2002.
- 1024 Singh, G., Wasson, R. J., and Agrawal, D. P.: Vegetational and seasonal climatic changes since
1025 the last full glacial in the Thar Desert, northwestern India, *Review of Palaeobotany and*
1026 *Palynology*, 64, 351-358, 1990.
- 1027 Sinha, R., Smykatz-Kloss, W., Stüben, D., Harrison, S. P., Berner, Z., and Kramar, U.: Late
1028 Quaternary palaeoclimatic reconstruction from the lacustrine sediments of the Sambhar
1029 playa core, Thar Desert margin, India, *Palaeogeography, Palaeoclimatology,*
1030 *Palaeoecology*, 233, 252-270, 2006.
- 1031 Sirocko, F.: Deep-sea sediments of the Arabian Sea: A paleoclimatic record of the
1032 southwest-Asian summer monsoon, *Geologische Rundschau*, 80, 557-566, 1991.
- 1033 Sonderegger, D. L., Wang, H., Clements, W. H., and Noon, B. R.: Using SiZer to detect
1034 thresholds in ecological data, *Frontiers in Ecology and the Environment*, 7, 190-195,
1035 2009.
- 1036 Staubwasser, M., Sirocko, F., Grootes, P. M., and Erlenkeuser, H.: South Asian monsoon
1037 climate change and radiocarbon in the Arabian Sea during early and middle Holocene,
1038 *Paleoceanography and Paleoclimatology*, 17, 2002.
- 1039 Staubwasser, M., Sirocko, F., Grootes, P. M., and Segl, M.: Climate change at the 4.2 ka BP
1040 termination of the Indus valley civilization and Holocene south Asian monsoon variability,
1041 *Geophysical Research Letters*, 30, 2003.
- 1042 Staubwasser, M., and Weiss, H.: Holocene climate and cultural evolution in late prehistoric-
1043 early historic West Asia, *Quaternary Research*, 66, 372-387, 2006.
- 1044 Staubwasser, M.: Late Holocene Drought Pattern Over West Asia. *Climates, Landscapes, and*
1045 *Civilizations*, 89-96, 2012.
- 1046 Steinke, S., Mohtadi, M., Groeneveld, J., Lin, L. C., Löwemark, L., Chen, M. T., and Rendle-
1047 Bühring, R.: Reconstructing the southern South China Sea upper water column structure
1048 since the Last Glacial Maximum: Implications for the East Asian winter monsoon
1049 development, *Paleoceanography and Paleoclimatology*, 25, 2010.
- 1050 Steph, S., Regenber, M., Tiedemann, R., Mulitza, S., and Nürnberg, D.: Stable isotopes of
1051 planktonic foraminifera from tropical Atlantic/Caribbean core-tops: Implications for
1052 reconstructing upper ocean stratification. *Marine Micropaleontology*, 71, 1-19, 2009.
- 1053 Tian, J., Wang, P., Chen, R., and Cheng, X.: Quaternary upper ocean thermal gradient
1054 variations in the South China Sea: Implications for east Asian monsoon climate,
1055 *Paleoceanography*, 20, 2005.
- 1056 Von Rad, U., Schulz, H., Khan, A. A., Ansari, M., Berner, U., Čepek, P., Cowie, G., Dietrich, P.,
1057 Erlenkeuser, H., Geyh, M., Jennerjahn, T., Lückge, A., Marchig, V., Riech, V., Rösch, H.,
1058 Schäfer, P., Schulte, S., Sirocko, F., and Tahir, M.: Sampling the oxygen minimum zone off
1059 Pakistan: glacial-interglacial variations of anoxia and productivity (preliminary results,
1060 SONNE 90 cruise), *Marine Geology*, 125, 7-19, 1995.
- 1061 Von Rad, U.: Physical oceanography during SONNE cruise SO90, PANGAEA,
1062 doi:10.1594/PANGAEA.805802, 2013.
- 1063 Walker, M. J., Berkelhammer, M., Björck, S., Cwynar, L. C., Fisher, D. A., Long, A. J., Lowe, J.
1064 J., Newnham, R. M., Rasmussen, S. O., and Weiss, H.: Formal subdivision of the Holocene

1065 Series/Epoch: a Discussion Paper by a Working Group of INTIMATE (Integration of ice-
1066 core, marine and terrestrial records) and the Subcommittee on Quaternary Stratigraphy
1067 (International Commission on Stratigraphy), *Journal of Quaternary Science*, 27, 649-659,
1068 2012.

1069 Wang, L., Sarnthein, M., Duplessy, J. C., Erlenkeuser, H., Jung, S., and Pflaumann, U.: Paleo
1070 sea surface salinities in the low-latitude Atlantic: The $\delta^{18}\text{O}$ record of *Globigerinoides*
1071 *ruber* (white), *Paleoceanography*, 10, 749-761, 1995.

1072 Wanner, H., Beer, J., Bütikofer, J., Crowley, T. J., Cubasch, U., Flückiger, J., Goosse, H.,
1073 Grosjean, M., Joos, F., Kaplan, J. O., Küttel, M., Müller, S. A., Prentice, C., Solomina, O.,
1074 Stocker, T. F., Tarasov, P., Wagner, M., and Widmann, M.: Mid-to Late Holocene climate
1075 change: an overview, *Quaternary Science Reviews*, 27, 1791-1828, 2008.

1076 [Weatherall, P., Marks, K., Jakobsson, M., Schmitt, T., Tani, S., Arndt, J. E., Rovere, M.,
1077 Chayes, D., Ferrini, V., and Wigley, R.: A new digital bathymetric model of the world's
1078 oceans, *Earth and Space Science*, 2, 331-345, 2015.](#)

1079 Weber, S.: Seeds of urbanism: palaeoethnobotany and the Indus Civilization, *Antiquity*, 73,
1080 813-826, 1999.

1081 Weber, S. A.: Archaeobotany at Harappa: indications for change, *Indus ethnobiology: new
1082 perspectives from the field*, 175-198, 2003.

1083 Weber, S. A., Barela, T., and Lehman, H.: Ecological continuity: An explanation for
1084 agricultural diversity in the Indus Civilization and beyond, *Man and Environment*, 35, 62-
1085 75, 2010.

1086 Weiss, H.: Global megadrought, societal collapse and resilience at 4.2-3.9 ka BP across the
1087 Mediterranean and West Asia, *Clim. Chang. Cult. Evol, PAGES Mag*, 24, 62, 2016.

1088 ~~Wheeler, M.: *The Indus Civilization*, Cambridge University Press, Great Britain, 1968.~~

1089 Wick, L., Lemcke, G., and Sturm, M.: Evidence of Lateglacial and Holocene climatic change
1090 and human impact in eastern Anatolia: high-resolution pollen, charcoal, isotopic and
1091 geochemical records from the laminated sediments of Lake Van, Turkey. *The Holocene*,
1092 13, 665-675, 2003.

1093 Wright, R. P.: *The ancient Indus: urbanism, economy, and society*, Cambridge University
1094 Press, Great Britain, 107, 2010.

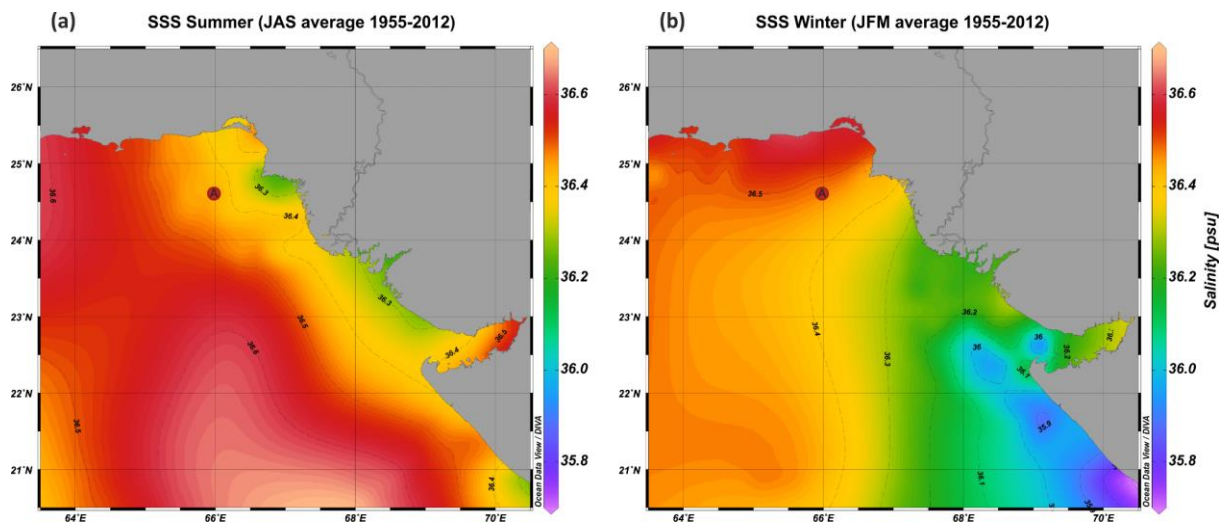
1095 Yadav, R. K., Kumar, K. R., and Rajeevan, M.: Characteristic features of winter precipitation
1096 and its variability over northwest India. *J. Earth Syst. Sci.*, 121, 611-623, 2012.

1097 Yu, W., Yang, Y. C., Savitsky, A., Alford, D., Brown, C., Wescoat, J., Debowicz, D., and
1098 Robinson, S.: *The Indus basin of Pakistan: The impacts of climate risks on water and
1099 agriculture*, The World Bank, 2013.

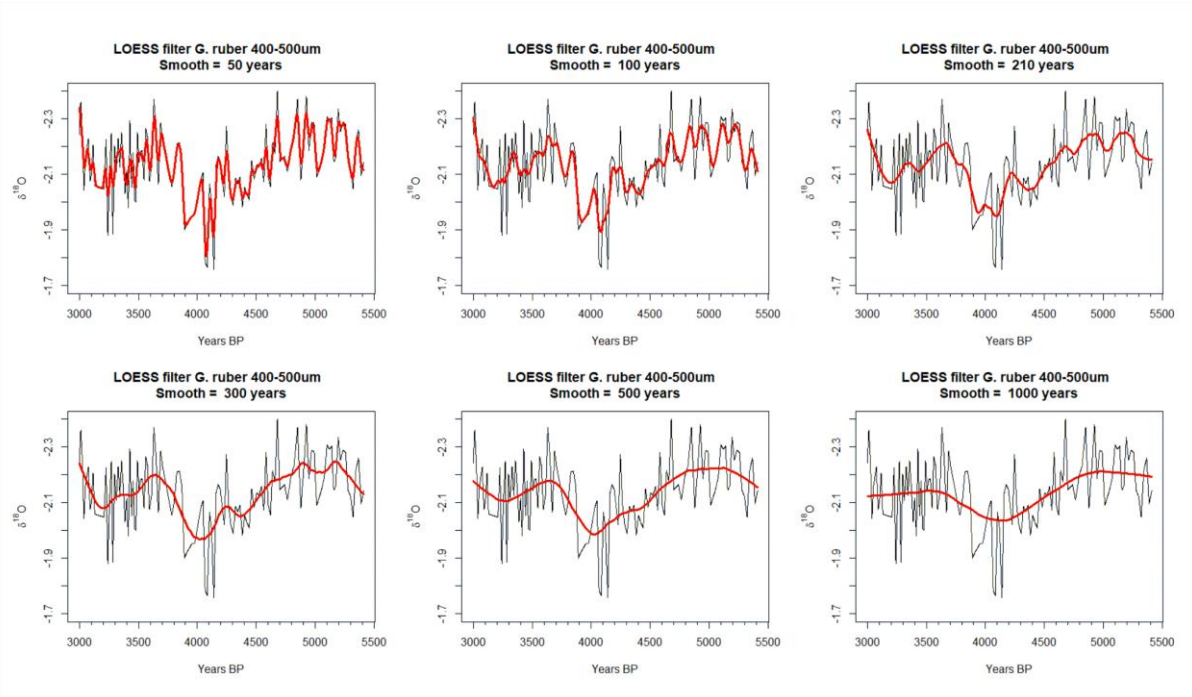
1100 Zaric, S.: Planktic foraminiferal flux of sediment trap EAST-86/90_trap, PANGAEA, doi:
1101 10.1594/PANGAEA.264508, 2005.

1102 Zweng, M. M., Reagan, J. R., Antonov, J. I., Locarnini, R. A., Mishonov, A. V., Boyer, T. P.,
1103 Garcia, H. E., Baranova, O. K., Johnson, D. R., Seidov, D., and Biddle, M. M.: *World Ocean
1104 Atlas 2013, Volume 2: Salinity*. Levitus, S. (Ed.), Mishonov, A. (Technical Ed.), NOAA Atlas
1105 NESDIS 74, 39, 2013.

1106 Supplemental figures and tables
1107

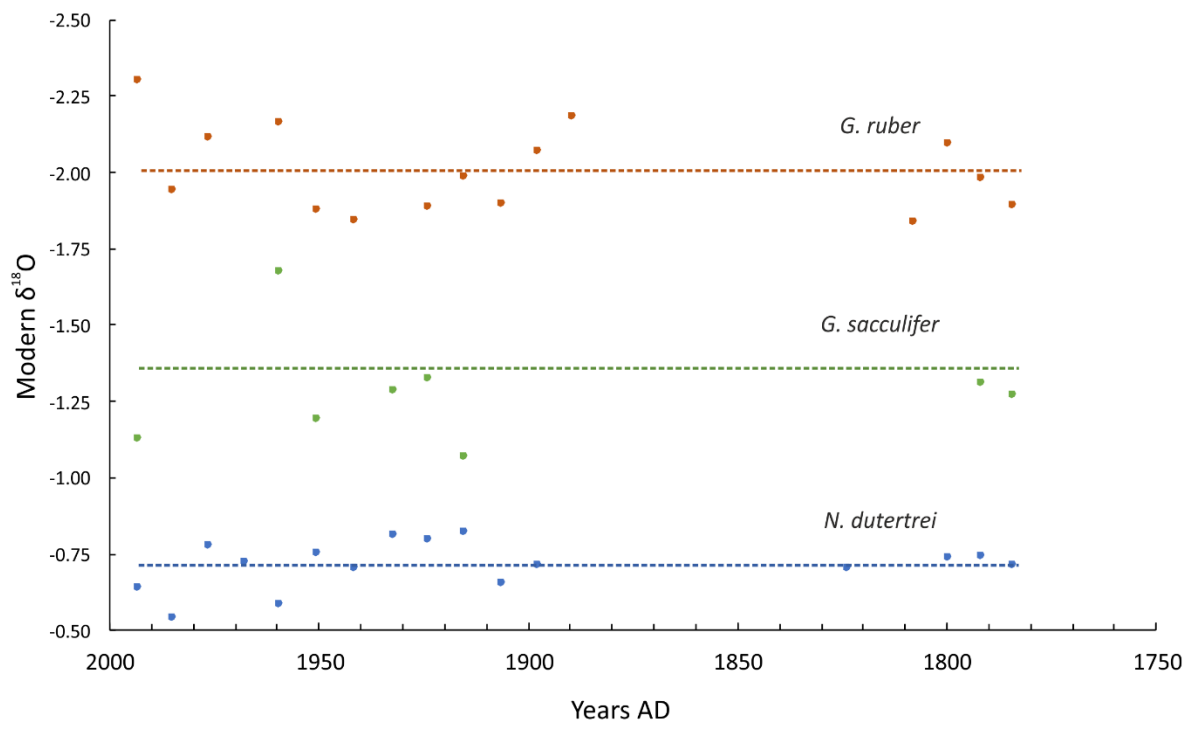


1108 **Figure S1.** Mean surface salinity for 1955-2012, with data from the 2013 World Ocean Atlas (WOA) at
1109 0.25° resolution (Zweng et al., 2013). Salinity contours are shown for **a.** summer (JAS) and **b.** winter
1110 (JFM). The Indus River is outlined. Note that over the time window of this dataset, modern Indus River
1111 discharge has been reduced by >50% due to barrages and irrigation (Ahmad et al., 2001). Plots created
1112 with Ocean Data Viewer (ODV).
1113
1114



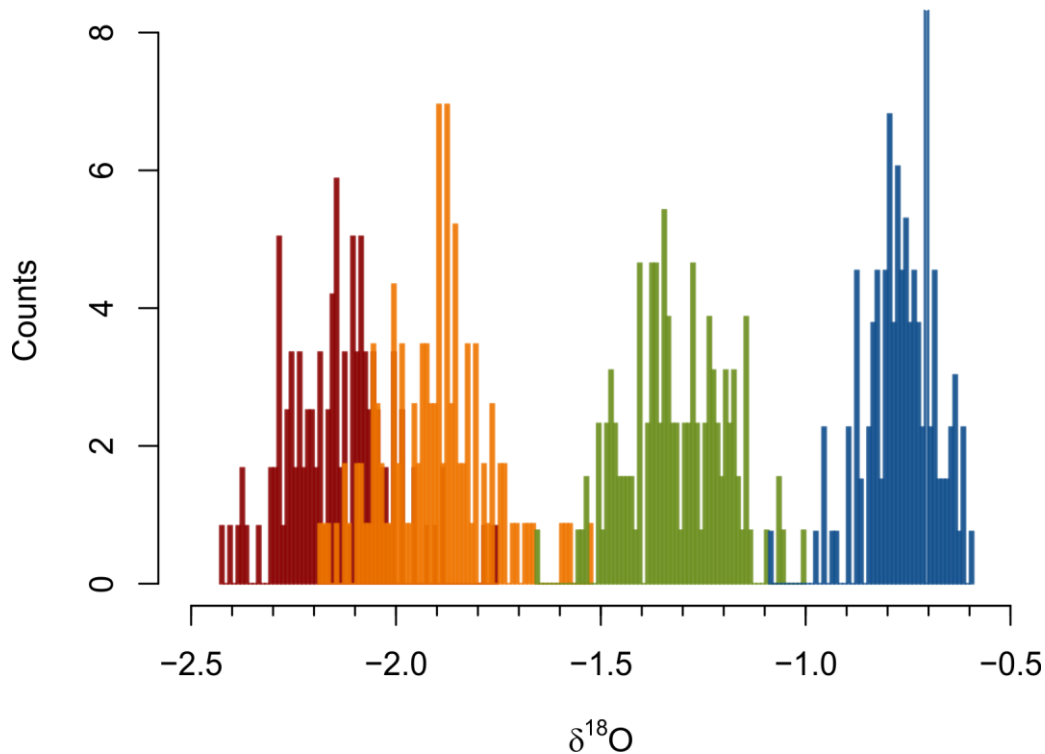
1115
1116
1117
1118
1119

Figure S2. Comparison of loess smoothing windows of 50, 100, 210, 300, 500, and 1000 years for *G. ruber* in the 400-500 μ m fraction.

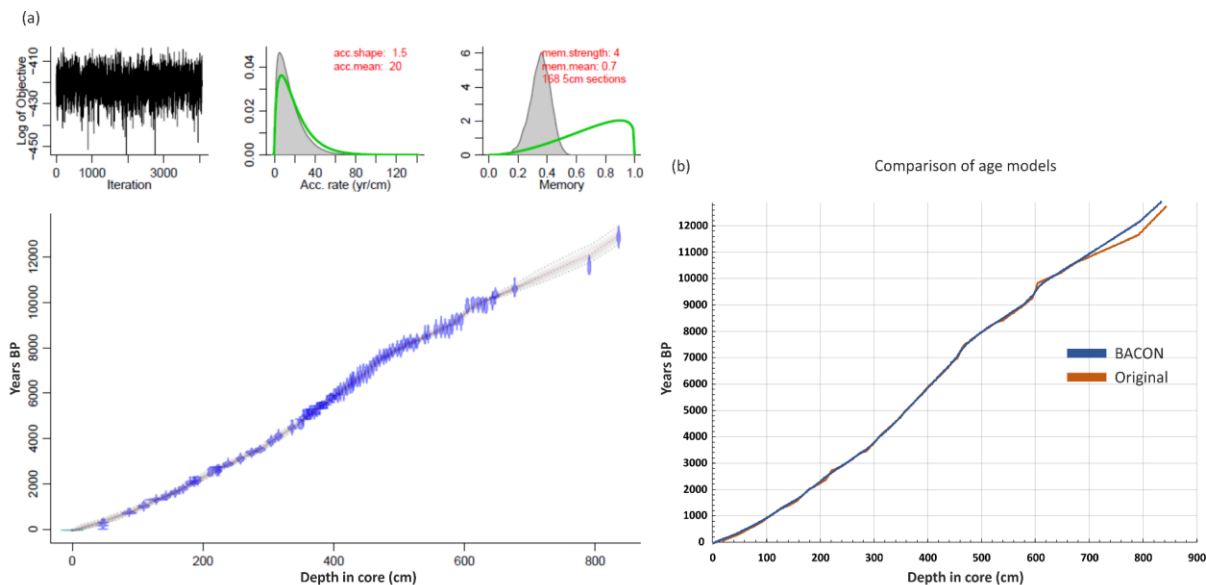


1120
1121
1122
1123
1124
1125
1126

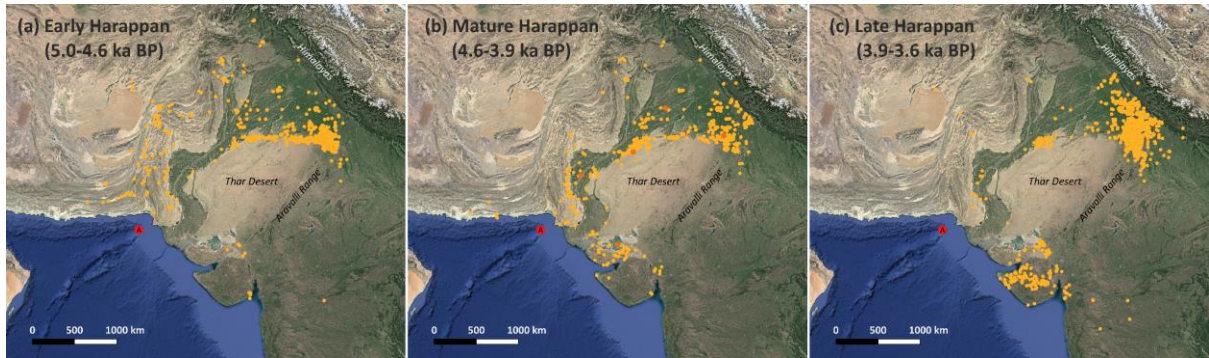
Figure S3. Modern $\delta^{18}\text{O}$ values of calcite, spanning approximately the last 200 years, measured from surface sediment samples for all three species at the size fractions 315-400 μ m. Averages values for the last 200 years (\sim 1780-1993 AD) are compared to the period 5.4-3.0 ka BP: -2.01‰ (modern) and -1.90‰ (old) for *G. ruber* (orange), -1.28‰ (modern) and -1.31‰ (old) for *G. sacculifer* (green), and -0.72‰ (modern) and -0.76‰ (old) for *N. dutertrei* (blue).



1127 $\delta^{18}\text{O}$
 1128 **Figure S4.** Frequency distributions of $\delta^{18}\text{O}$ data during 5.4-3.0 ka BP for *G. ruber* 400-500 μm (red), *G.*
 1129 *ruber* 315-400 μm (orange), *G. sacculifer* 315-400 μm (green), *N. dutertrei* 315-400 μm (blue).
 1130



1131 **Figure S5. a.** BACON age-depth model with calibrated dates shown in blue **b.** Age-depth model
 1132 comparison with the original published age model from Staubwasser et al. (2003) (orange) and the
 1133 new age model based on BACON software (blue).
 1134
 1135



1136
1137
1138
1139
1140
1141
1142
1143
1144

Figure S6. Indus site distributions (yellow points) during the **a.** Early Harappan (~5.0-4.6 ka BP), **b.** Mature Harappan (~4.6-3.9 ka BP), and **c.** Late Harappan (~3.9-3.6 ka BP). Orange sites show larger Harappan cities during the Mature Harappan period (Dholavira, Mohenjo Daro, Ganweriwala, Harappa, and Rakhigarhi from bottom to top), core 63KA shown by red circle, background terrain from Google Earth.

Table S1. Main statistical parameters of the $\delta^{18}\text{O}$ data.

	<i>G. ruber</i> 400-500 μm	<i>G. ruber</i> 315-400 μm	<i>G. sacculifer</i> 315-400 μm	<i>N. dutertrei</i> 315-400 μm
<i>n</i>	119	115	129	132
<i>Minimum</i>	-2.423	-2.190	-1.660	-1.090
<i>Maximum</i>	-1.752	-1.520	-1.000	-0.590
<i>1st Quartile</i>	-2.232	-1.995	-1.400	-0.810
<i>3rd Quartile</i>	-2.068	-1.830	-1.220	-0.700
<i>Mean</i>	-2.139	-1.901	-1.312	-0.761
<i>Median</i>	-2.144	-1.890	-1.320	-0.760
<i>Sum</i>	-254.58	-218.66	-169.26	-100.46
<i>SE Mean</i>	0.012	0.012	0.011	0.007
<i>LCL Mean</i>	-2.163	-1.926	-1.333	-0.776
<i>UCL Mean</i>	-2.116	-1.877	-1.291	-0.746
<i>Variance</i>	0.016	0.017	0.015	0.007
<i>Stdev</i>	0.128	0.131	0.122	0.085
<i>Skewness</i>	0.408	0.288	-0.011	-0.592
<i>Kurtosis</i>	0.511	0.174	-0.364	0.850

1145
1146
1147

Table S2. Age-Model calibration with BACON software.

<i>Depth (cm)</i>	<i>¹⁴C date</i>	<i>Error ($\pm 1\sigma$)</i>	<i>Reservoir (years)</i>	<i>IntCal13 min age BP</i>	<i>IntCal13 max age BP</i>	<i>IntCal13 mean age BP</i>
<i>surface</i>	-	-	-	-	-	-43
47	790	30	565	267	309	288
87	1370	35	565	678	780	729
109.5	1665	30	565	952	1062	1007
128.5	1955	25	565	1283	1339	1311
143.5	2115	35	565	1369	1529	1449
157.5	2270	25	565	1552	1634	1593
169.5	2430	25	565	1728	1869	1799
180.5	2640	25	565	1988	2122	2055
186.5	2675	35	565	1993	2154	2074
191.5	2720	30	565	2044	2184	2114
211.5	3000	35	565	2356	2541	2449

221.5	3110	40	565	2491	2602	2547
224.5	3145	25	565	2708	2758	2733
238.5	3340	25	565	2836	2929	2883
257.5	3510	30	565	2999	3181	3090
274.5	3730	30	565	3343	3451	3397
287.5	3850	30	565	3450	3576	3513
304.5	4145	30	565	3828	3975	3902
315.5	4310	30	565	4062	4159	4111
336.5	4570	40	565	4408	4578	4493
349.5	4655	40	565	4512	4711	4612
353.5	4870	30	565	4832	4892	4862
357.5	5005	35	565	4952	5079	5016
360.5	4980	30	565	4868	5057	4963
363.5	5080	30	565	5050	5194	5122
366.5	5105	35	565	5053	5189	5121
370.5	5070	35	565	5046	5300	5173
374.5	5160	40	565	5372	5463	5418
378.5	5210	40	565	5303	5469	5386
381.5	5315	30	565	5460	5585	5523
385.5	5315	35	565	5453	5586	5520
389.5	5420	35	565	5580	5654	5617
395.5	5635	35	565	5741	5907	5824
398.5	5610	35	565	5713	5904	5809
402	5750	40	565	5891	6008	5950
406.5	5830	35	638	5899	6002	5951
410.5	5965	40	638	5994	6210	6102
415.5	5980	45	638	5997	6216	6107
420.5	6120	45	638	6201	6351	6276
425.5	6265	45	638	6311	6490	6401
428.5	6335	55	638	6395	6639	6517
430.5	6345	60	638	6396	6657	6527
436.5	6440	40	638	6495	6678	6587
440.5	6540	55	638	6627	6883	6755
445.5	6665	45	638	6773	6984	6879
450.5	6650	40	638	6749	6948	6849
455.5	6960	45	824	6912	7162	7037
460.5	7155	45	824	7166	7331	7249
465.5	7310	45	824	7308	7480	7394
470.5	7480	55	824	7438	7606	7522
476.5	7550	50	824	7551	7670	7611
480.5	7815	55	1011	7571	7743	7657
485.5	7920	70	1011	7617	7867	7742
490.5	8070	50	1011	7788	7976	7882
497.5	8130	55	1011	7837	8027	7932
502.5	8115	55	1011	7828	8020	7924
507.5	8400	60	1011	8148	8345	8247

512.5	8350	50	1011	8020	8218	8119
517.5	8490	50	1011	8194	8381	8288
522.5	8355	60	1011	8023	8312	8168
527.5	8510	60	1011	8194	8400	8297
539.5	8790	60	1118	8384	8563	8474
544.5	8880	55	1118	8425	8631	8528
556.5	9060	50	1118	8637	8986	8812
564.5	9120	70	1118	8636	9026	8831
570.5	9110	50	1118	8698	9007	8853
576.5	9060	50	1118	8637	8986	8812
581.5	9260	50	1118	8999	9153	9076
588.5	9390	50	1118	9119	9430	9275
595	9370	60	1118	9076	9419	9248
604.5	9570	50	781	9602	9952	9777
613	9660	70	781	9736	10194	9965
621.5	9670	50	781	9884	10189	10037
628	9650	70	781	9732	10188	9960
633	9570	80	781	9581	9963	9772
643	9770	70	781	9906	10251	10079
647.5	9920	60	781	10206	10436	10321
677	10160	60	781	10480	10752	10616
791	11145	50	1095	11325	11806	11566
836	12285	55	1300	12726	12995	12861